# Unravelling the Mechanism of the Asymmetric Hydrogenation of Acetophenone by [RuX$_2$(diphosphine)(1,2-diamine)] Catalysts

Pavel A. Dub,*,[†] Neil J. Henson,[‡] Richard L. Martin,[‡] and John C. Gordon*,[†]

[†]Chemistry Division, MS J582, and [‡]Theoretical Division, MS B268, Los Alamos National Laboratory, Los Alamos, New Mexico 87545, United States

Ⓢ *Supporting Information*

ABSTRACT: The mechanism of catalytic hydrogenation of acetophenone by the chiral complex *trans*-[RuCl$_2${(S)-binap}{(S,S)-dpen}] and KO-*t*-C$_4$H$_9$ in propan-2-ol is revised on the basis of DFT computations carried out in dielectric continuum and the most recent experimental observations. The results of these collective studies suggest that neither a six-membered pericyclic transition state nor any multibond concerted transition states are involved. Instead, a hydride moiety is transferred in an outer-sphere manner to afford an ion-pair, and the corresponding transition state is both enantio- and rate-determining. Heterolytic dihydrogen cleavage proceeds neither by a (two-bond) concerted, four-membered transition state, nor by a (three-bond) concerted, six-membered transition state mediated by a solvent molecule. Instead, cleavage of the H−H bond is achieved via deprotonation of the η^2-H$_2$ ligand within a cationic Ru complex by the chiral conjugate base of (R)-1-phenylethanol. Thus, protonation of the generated (R)-1-phenylethoxide anion originates from the η^2-H$_2$ ligand of the cationic Ru complex and not from NH protons of a neutral Ru *trans*-dihydride complex, as initially suggested within the framework of a metal−ligand bifunctional mechanism. Detailed computational analysis reveals that the 16e$^-$ Ru amido complex [RuH{(S)-binap}{(S,S)-HN-(CHPh)$_2$NH$_2$}] and the 18e$^-$ Ru alkoxo complex *trans*-[RuH{OCH(CH$_3$)(R)}{(S)-binap}{(S,S)-dpen}] (R = CH$_3$ or C$_6$H$_5$) are not intermediates within the catalytic cycle, but rather are off-loop species. The accelerative effect of KO-*t*-C$_4$H$_9$ is explained by the reversible formation of the potassium amidato complexes *trans*-[RuH$_2${(S)-binap}{(S,S)-N(K)H-(CHPh)$_2$NH$_2$}] or *trans*-[RuH$_2${(S)-binap}{(S,S)-N(K)H(CHPh)$_2$NH(K)}]. The three-dimensional (3D) cavity observed within these molecules results in a chiral pocket stabilized via several different noncovalent interactions, including neutral and ionic hydrogen bonding, cation−π interactions, and π−π stacking interactions. Cooperatively, these interactions modify the catalyst structure, in turn lowering the relative activation barrier of hydride transfer by ∼1−2 kcal mol^{-1} and the following H−H bond cleavage by ∼10 kcal mol^{-1}, respectively. A combined computational study and analysis of recent experimental data of the reaction pool results in new mechanistic insight into the catalytic cycle for hydrogenation of acetophenone by Noyori's catalyst, in the presence or absence of KO-*t*-C$_4$H$_9$.
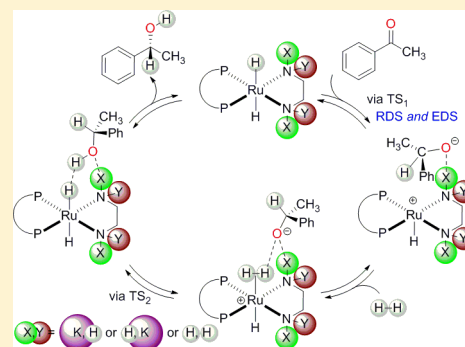
1. INTRODUCTION

Since the pioneering work of Noyori, Ikariya, Ohkuma, and co-workers, the ruthenium (Ru)-catalyzed asymmetric hydrogenation of acetophenone and other aromatic or simple ketones has become a powerful, practical, and environmentally benign tool for preparing chiral secondary alcohols with high optical purities.[1] A number of different (pre)catalysts of the type *trans*-[RuCl$_2${(S)-diphosphine}{(S,S)-dpen}][2] (diphosphine = binap **1a**,[1a,e] tolbinap **1b**,[1a,e] xylbinap **1c**[1g]), *trans*-[RuCl$_2${(S)-xylbinap}{(S)-daipen}] **1d**,[1g] or [RuCl{(S)-xylbinap}{(S)-daipena}] **1e**[3] have been explored in this regard. These systems have typically exhibited the highest activities in propan-2-ol and in the presence of large excesses of base such as KOH, KO-*i*-C$_3$H$_7$, or KO-*t*-C$_4$H$_9$ (ca. 10−500 equiv and up to 24 000). Currently, enantioselective ketone hydrogenation represents one of the most powerful class of homogeneously catalyzed reactions discovered so far,[4] exhibiting substrate-to-catalyst ratios (S/C) in the range of thousands up to a few million.

The highly diastereo-, enantio-, and chemoselective hydrogenation of C═O versus C═C typically requires 5−45 atm of H$_2$, moderate temperatures (25−40 °C), and, in the case of acetophenone, provides (R)-1-phenylethanol quantitatively within several hours (up to 60 h) with good to excellent enantioselectivities (from 80% to >99% ee's).[5] Hydrogenation with high S/C = 100 000[1g] and 2 400 000,[1e] respectively, was only practical when extremely large amounts of base were present in the reaction mixture (Ru/KO-*t*-C$_4$H$_9$ = 400 and 24 000, respectively). Catalytic reaction may proceed in the absence of base with the same reported degree of enantioselectivity. This is the case with precatalysts *trans*-[RuH(η^1-BH$_4$){(S)-tolbinap}{(S,S)-dpen}] **1f** or *trans*-[RuH-

Scheme 1. Currently Accepted Catalytic Cycles for the Hydrogenation of Acetophenone (or Other Aromatic Ketones) by [RuX$_2$(diphosphine)(1,2-diamine)]: Catalytic Cycle I (Base-Free Conditions), Catalytic Cycle II (under High Base Concentration)[a]
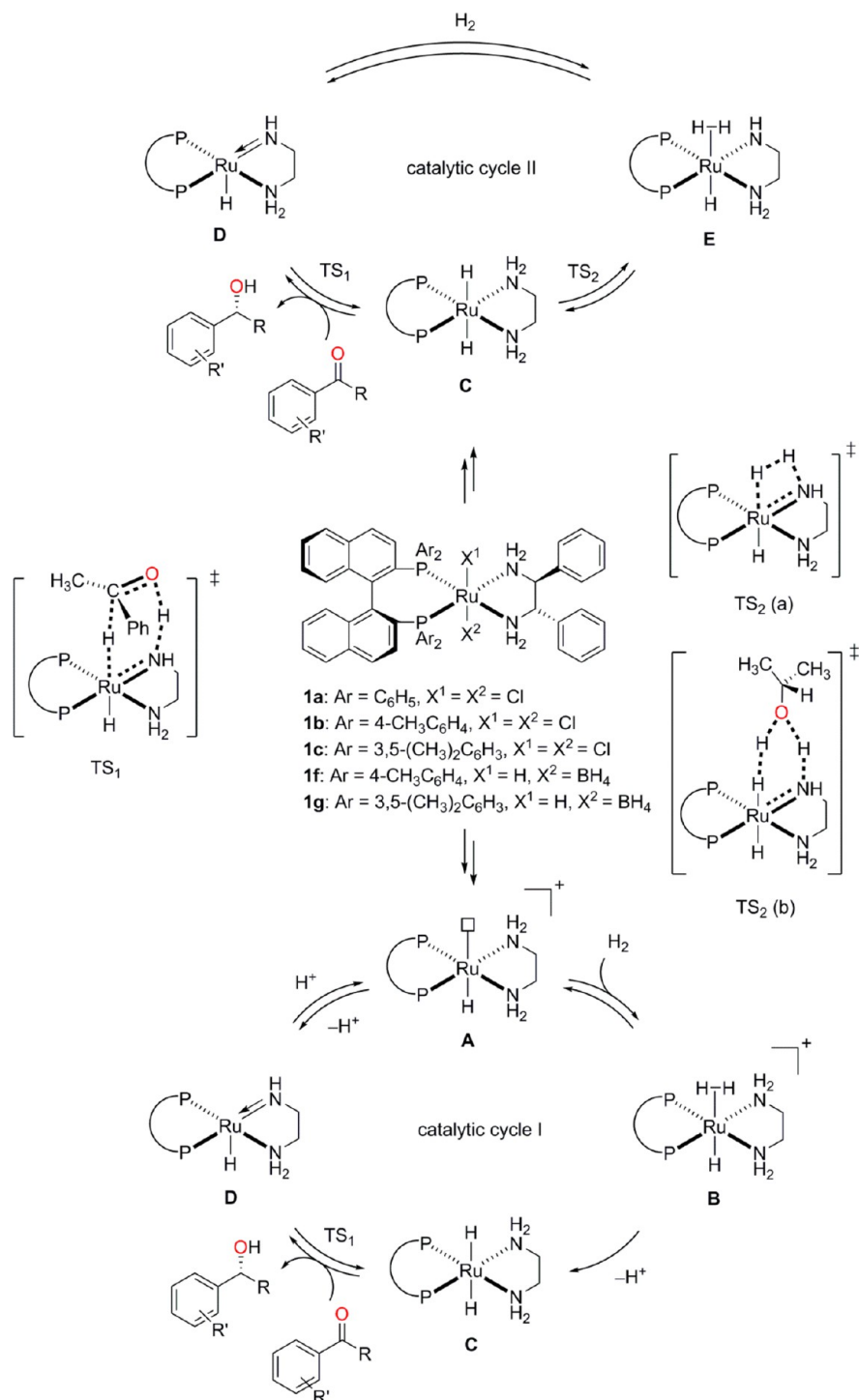
[a]Formation of the major enantiomeric product is shown.

(η^1-BH$_4$){(S)-xylbinap}{(S,S)-dpen}] **1g**.[6] However, the reaction rate was significantly lower (by at least 1 order of magnitude) as compared to that in the presence of added base.[6,7] Industrial applications with the more robust and stable chiral complex *trans*-[RuCl$_2$(diphosphine)(1,2-diamine)] or its derivatives employ large amounts of base.[8] For example, the catalytic enantioselective synthesis of taranabant at Merck utilizes **1d** and 130 equiv of KO-*t*-C$_4$H$_9$ (20% relative to the substrate).[9] The exact role that the base plays is not clearly understood thus far.

Initially, the presence of a base was considered essential for neutralizing HCl formed during dehydrochlorination of precatalyst **1** resulting in the catalytic, *trans*-RuH$_2$ complex.[5b] The induction period indicated by kinetic studies was

considered to support this explanation.[7,10] Additionally, the role of base in small concentrations was explained as necessary for the catalytic cycle to accelerate the deprotonation of the η^2-H_2 ligand from the putative cationic Ru complex (Scheme 1, catalytic cycle I, complex **B**), which was accepted as a "rate-determining step".[7,10] Later, Bergens et al. proposed that a stoichiometric amount of base is required to regenerate the catalyst from the alkoxo Ru complex that was intercepted in the reaction mixture.[11] These explanations, however, did not rationalize why only a large excess of base accelerates the reaction. On the other hand, Hartmann and Chen clearly and conclusively demonstrated experimentally that an alkali cation (or more generally, a Lewis acid), rather than a base itself ($^-$OR, R = -t-C_4H_9), was needed for turnover.[12] After more than 10 years, this experimental finding still has not been rationalized adequately in the context of understanding the catalytic hydrogenation cycle.

Two catalytic cycles have been proposed for the hydrogenation of aromatic ketones by [RuX$_2$(diphosphine)(1,2-diamine)] (X = Cl or other ligands) based on stoichiometric experiments, isotope effects, and kinetics, typically probed via NMR spectroscopy, a detection method with a relatively slow time scale (Scheme 1).[7,13] Either mechanism, or both, may be in operation, depending on the reaction conditions, the nature of solvent, and notably the presence or absence of base. Under base-free conditions in propan-2-ol, or when small amounts of base are employed, catalytic cycle I is proposed to be dominant[14] as shown in Scheme 1. In such a scenario, precatalyst **1** is transformed into cationic complex **A** (or its Werner-type solvate), which upon reversible deprotonation forms the 16e$^-$ Ru amido complex **D**. Cationic 16e$^-$ complex **A** reacts with H$_2$ reversibly to form the 18e$^-$ complex **B** (a possible resting state), which undergoes rate-determining deprotonation of the η^2-H_2 ligand by the solvent (acting as an ambient base) to generate the 16e$^-$ Ru dihydride **C**. Irreversible, rapid reaction of **C** with acetophenone provides, via the enantiodetermining step (EDS), 16e$^-$ complex **D** and the chiral alcohol. This reaction was postulated to proceed via a six-membered pericyclic transition state **TS$_1$**, giving rise to the term "metal–ligand bifunctional mechanism".[10] Protonation of the nitrogen atom of **D** by alcohol solvent regenerates **A**, completing catalytic cycle I.

Alternatively, **C** can also be regenerated from **D** (resting state) by way of complex **E** via **TS$_2$** (designated as a rate-determining step), enabling catalytic cycle II as shown Scheme 1.[7] This cycle was proposed to be dominant under conditions of high base concentration in propan-2-ol, or in nonalcoholic solvents, where some activity was also observed (typically in the presence of base). The operation of catalytic cycle II in aprotic solvents (neat ketones, benzene) was also suggested by Morris et al., where the (pre)catalyst was chiral trans-[RuXCl-(diphosphine)(1,2-diamine)], X = Cl or H.[15]

Both catalytic cycles are similar in three regards: (a) proposed intermediates (**C** and **D**), (b) cleavage of dihydrogen was formulated as a "rate-determining step", and (c) a similar EDS that occurs via a six-membered pericyclic transition state **TS$_1$**. In this transition state structure, delivery of a hydride moiety from the Ru center and a proton from the NH$_2$ ligand to the ketone takes place simultaneously, yielding alcohols without forming Ru alkoxide intermediates.[7] The entrenched pericyclic mechanism is still extensively accepted in the literature and appears in recent reviews[4b,16] and other publications.[17]

The difference between each cycle in Scheme 1 relates to the manner in which molecular hydrogen is cleaved. Much less attention has been devoted to discussion of this step, except for numerous computational modeling studies of **TS$_2$**. The H–H bond is cleaved either via a (two-bond) four-membered concerted transition state **TS$_2$(a)** or via a concerted (three-bond) six-membered solvent-mediated proton shuttle, **TS$_2$(b)**. In 2005, using a simplified computational model, Brandt and Andersson demonstrated that a transition state of type **TS$_2$(a)** is 12.7 kcal mol^{-1} less favorable than a transition state of the type **TS$_2$(b)**, which corresponds to the computed concerted transition state structure in the gas phase.[18] Despite this fact, **TS$_2$(a)** is still considered to be the key pathway to cleave molecular hydrogen.[15a,17b,c,i,19] It was suggested[20] that **TS$_2$(a)** may occur on an excited state; however, the computed energy difference is only 4.5 kcal mol^{-1} in continuum propan-2-ol, which is still higher than **TS$_2$(b)**. The typically computed relative activation energy for **TS$_2$(a)** of 25 kcal mol^{-1}, or even an excited state value of 19 kcal mol^{-1}, rather suggests that the reaction does not proceed via this pathway (the experimental initial TOF[21] is estimated to be 583 s^{-1} for **1e** after 2–3 min,[3] or 63 s^{-1} for **1b** at 30% conversion and 30 °C[1e]).

A series of NMR experiments from Bergens' group[11,22] are inconsistent with the presently accepted mechanisms (Scheme 2) as follows: (a) addition of acetophenone (or other ketones) to the trans-dihydride complex **C** at low temperature (THF-d_8, −80 °C, 2 atm H$_2$) generated the alkoxide complex trans-[RuH(OCHPhMe){S,S-binap}{S-dpen}] (**F**) exclusively as a kinetic product, and not amido Ru complex **D** plus 1-phenylethanol as expected from a pericyclic reaction;[22a,b] (b)

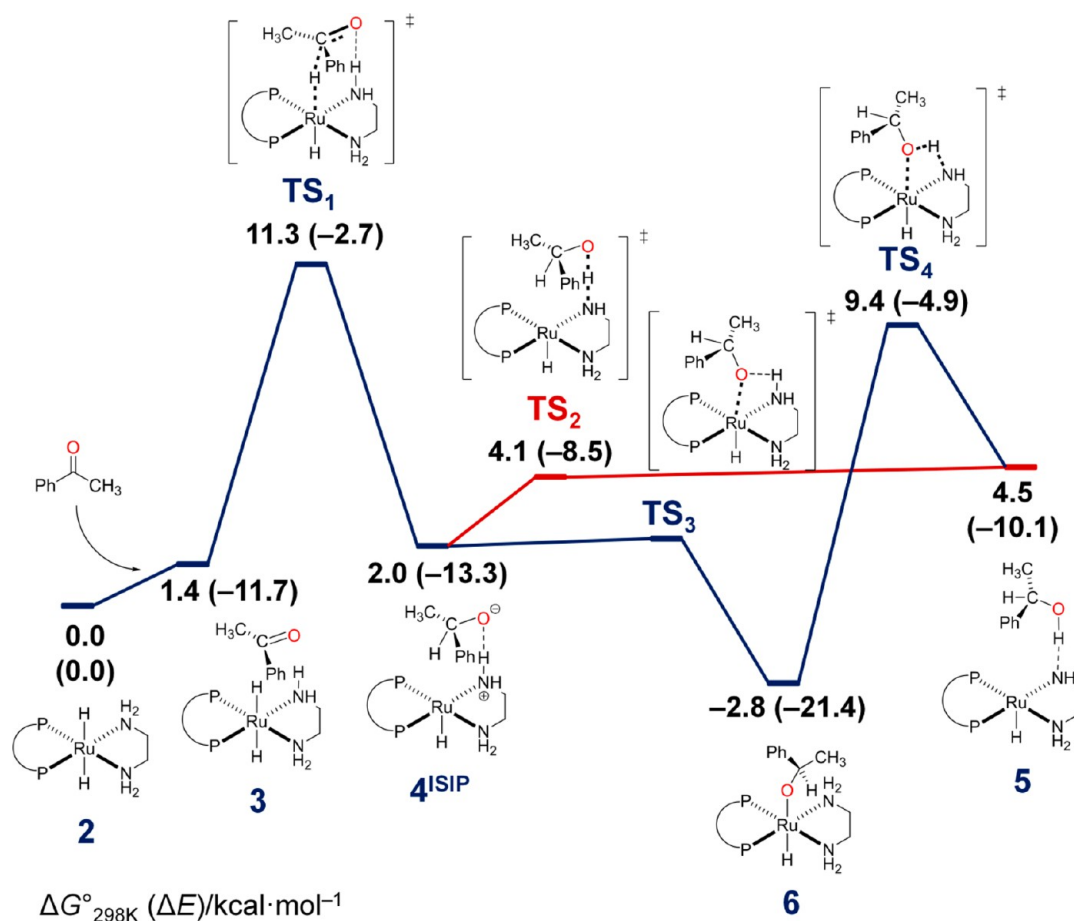**Scheme 2. Experimental Results of Bergens et al. Inconsistent with the Accepted Mechanisms[11,22]**
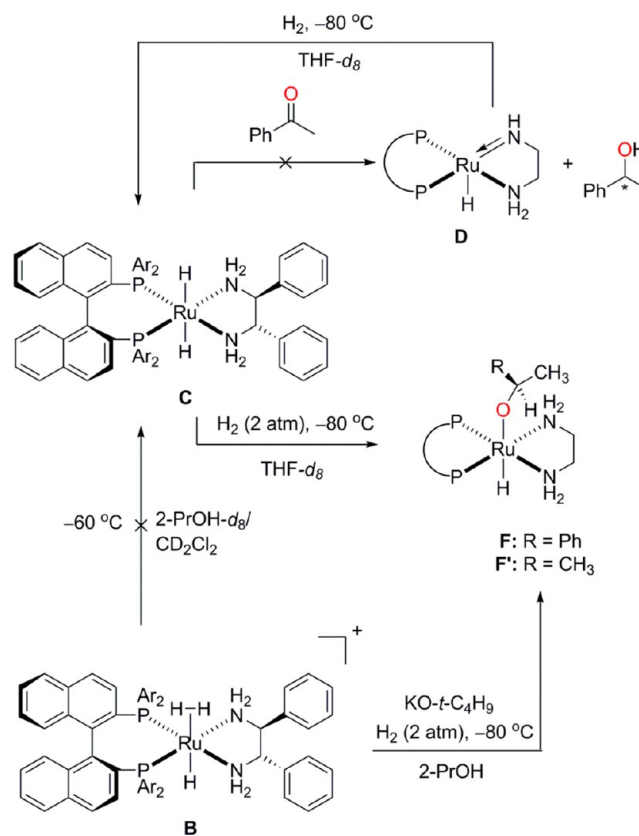
Figure 1. DFT/ωB97X-D/SDD(Ru)/6-31G*(C,H,N,O,P)/SMD(propan-2-ol) energy profile of the enantioselective reaction between *trans*-[RuH$_2${(S)-binap}{(S,S)-dpen}] **2** and acetophenone. The formation of the major enantiomeric product is shown.

the kinetic and thermodynamic acidity of *trans*-[RuH(η^2-H$_2$){(R)-binap}{(R,R)-dpen}]$^+$BF$_4^-$ (**B·BF$_4$**) is insufficient to protonate propan-2-ol-d_8 at −60 °C;[22c] (c) in the absence of a base, **B·BF$_4$** did not generate sufficient active catalyst for the hydrogenation of acetophenone in propan-2-ol solvent (4 atm H$_2$, 30 °C, 2000 equiv of ketone, no base);[11,22c] (d) in the presence of a stoichiometric amount of base, precatalyst **B·BF$_4$** did successfully catalyze the hydrogenation of acetophenone; however, H−H cleavage from **B·BF$_4$** already occurred at −80 °C:[11] the product of this reaction was not intermediate **C** as expected from Scheme 1, but rather the isopropoxide complex *trans*-[RuH{OCHMe$_2$}{S,S-binap}{S-dpen}] (**F′**); and (e) addition of H$_2$ (∼2 atm) to amide complex of type **D** to produce **C** occurred at −80 °C (<5 min), although in THF-d_8.[11]

The simultaneous transfer of two hydrogen atoms via pericyclic transition state **TS$_1$** is the key concept of the presently accepted mechanism.[23] The pericyclic nature of **TS$_1$** has been supported by numerous gas-phase calculations. These types of gas-phase computations have utilized both simplified models as well as full models of **2** (Catlow,[17i,19a,b,24] Lei,[17c,h,25] and others[17b,d,19c]). Catalytic cycle II is typically promoted in these cases ad hoc, and transition state **TS$_1$** is found (normally together with **TS$_2$(a)**). Conversely, we[26] and others[20,27] have recently shown the reaction proceeds in solution in a stepwise fashion via high-energy ion-pair intermediates, which are not detectable by NMR spectroscopy.[26] The rationalization of this became possible after the introduction of a continuum solvent

reaction field,[20,26,28] explicit solvation,[27] or both[26] into calculations.

The purpose of this work is to present new detailed arguments and to show that they lead to a new outlook regarding the catalytic cycle for acetophenone hydrogenation by the active form of precatalyst **1a**, *trans*-[RuH$_2${(S)-binap}{(S,S)-dpen}] **2**, in the presence or absence of base in propan-2-ol. Our conclusions are based on large-scale density functional theory calculations performed in implicit solvent and backed up with known experimental results.

2. COMPUTATIONAL AND CONFORMATIONAL DETAILS

All calculations were carried out on unabridged chiral models[29] using code Gaussian 09[30] and the SMD polarizable continuum model[31] at the DFT[32]/ωB97X-D[33]/SDD(Ru)/6-31G*(C,H,N,O,P,K) level of theory. Geometry optimization and frequency calculations were performed in the continuum solvent reaction field of implicit propan-2-ol. Because of solute−solvent interactions, stationary and saddle points in solution phase usually do not correspond to stationary and saddle points in the gas phase.[34] This could be especially the true in the case of multibond[35] concerted reactions,[26,34] which chemists have traditionally felt free to postulate.[35] Previously, we and others have shown that different DFT combinations of functionals and continuum solvation models such as M06/SMD,[26] BLYP/C-PCM,[26] M06/PCM,[20] PBE0/PCM,[36] as well as Car−Parrinello Molecular Dynamics (CP-MD)[27] suggested that a one-bond concerted[35] reaction takes place, that is, cleavage and formation of one-bond, M−H (M = Ru, Os) and C−H, respectively, rather than a three-bond concerted[35] reaction occurring via a six-membered pericyclic transition state (PTS)

as typically found in the gas phase. Moreover, due to a high asynchronicity of this PTS, which should be described as corresponding to a two-stage concerted reaction,[35] even a slight change in the nature of the ketone,[37] its enantioface position relative to the reacting site (Re vs Si),[17b] or involvement of only one H-bonded solvent molecule[26] in the gas-phase calculations changed the potential energy surface (PES): first-order saddle point corresponding to the pericyclic transition state dissected into two saddle and one stationary point (high-energy intermediate) connecting them.

Recently, we found that the DFT combination of Head–Gordon's functional ωB97X-D with Truhlar's SMD continuum solvation model afforded reasonable results with high speed and accuracy.[28] The functional shows remarkable agreement with experimental thermochemistry for a number of reactions involving hydrogen interactions.[38] These benchmark studies typically utilized a basis (6-311++G**) much more extended than the 6-31G* basis set used here.[39] Nevertheless, as in our previous and similar studies with M06/SMD[26] or BLYP/C-PCM,[26] the nature of the PES (presence of stationary or saddle points), the qualitative outcomes of these results, and conclusions were independent of the use of a 6-31G* or 6-311++G** basis set. Single point calculations using the SDD+f(Ru)/6-311++G**(C,H,N,O,P,K) basis at a geometry found using the SDD(Ru)/6-31G*(C,H,N,O,P,K) basis have been performed for all stationary and saddle points presented in Figures 1, 3, and 5, and reported in Supporting Information Figures S1, S3, and S9, respectively. This will be denoted as SDD+f(Ru)/6-311++G**-(C,H,N,O,P,K)//SDD(Ru)/6-31G*(C,H,N,O,P,K).[40] A potential source of error is the use of a continuum solvent to assess the thermodynamics of ion pairs. A detailed investigation of this is warranted in the future, but at this point we note that we do not believe it would alter our conclusions.[41] Of note, SMD itself was applied to predict the free energy of solvation in ionic liquids.[42]

Unless otherwise noted, the molecular cavity was created as implemented in Gaussian 09. DFT integration grids with 99 radial and 590 angular points (Ultrafine) were used. The Gibbs free energies in continuum propan-2-ol, G (directly obtainable from output files under default T = 298.15 K, C = 1 atm[43] with the harmonic approximation and a scaling factor = 1.0), were then corrected as required in moving from the change of standard state[44] derived from the default concentration (1 atm) to the standard state in solution (1 M), by adding 0.00301 Hartree. Unless otherwise noted, the electronic (ΔE) or free energy (ΔG°_{298K}) in kcal mol^{-1} is calibrated relative to complex **2** and reagents. Intrinsic reaction coordinate (IRC)[45] calculations were computed for all of the transition states separately in the forward and reverse directions. All of the minima connected by any TS in this work were optimized from the IRC path. Molecular graphics images were produced using the UCSF Chimera package.[46] The turnover frequencies[21] (TOFs) were calculated by using the energetic span model approximation coined by Amatore[47] and extended by Shaik.[48] The kinetic isotope effects (KIEs) for single steps of IRC-obtained stationary points $\rightarrow$ first-order saddle point transformations for enantiodetermining hydride transfer (i.e., **3** $\rightarrow$ **TS$_1$**, **3–K^{ax}(a)** $\rightarrow$ **TS$_1$** **2–K^{ax}(a)**) or η^2–H$_2$ ligand H–H bond cleavage via deprotonation by (R)-1-phenylethoxide anion (i.e., **7** $\rightarrow$ **TS$_5$**, **7–K^{ax}(a)** $\rightarrow$ **TS$_5$** **2–K^{eq}(b)**) are presented in the Supporting Information.

Coordination of the binap ligand on the ruthenium center results in a conformationally rigid seven-membered chelate ring.[49] However, in the case of dpen ligand, there are two major conformations for the five-membered NN chelate ring that result from diamine coordination: λ, wherein hydrogen atoms of CH groups are located in axial (aa) positions, and δ, wherein hydrogens of CH groups are located in equatorial (ee) positions.[50] In all known X-ray structures[1e,15c,d] of chiral [RuX$_2$(diphosphine)(1,2-diamine)] complexes, the conformation of either seven- or five-membered rings was λ (in the case of the tmen ligand, C–Me groups were in axial positions). X ligands were located in trans-position. Because computations also show that the λ-conformer of trans-[RuH$_2${(S)-binap}{(S,S)-dpen}] (**2**) is 5.2 kcal mol^{-1} more stable than the δ-conformer, whereas the λ-conformer of potassium monoamidato complex trans-[RuH$_2${(S)-binap}{(S,S)-N-(K)HCHPhCHPhNH$_2$}] (**2–K^{eq}**, see below) is 6.8 kcal mol^{-1} more

stable than the δ-conformer on a free energy (ΔG_{298K}°) scale (Supporting Information Figure S2), we have restricted most of the subsequent analysis of computed catalytic cycles for complexes wherein both seven- and five-membered rings are in λ-conformations.

Morris' group has demonstrated that under base-free conditions, isolable trans-[RuHCl{(S)-binap}{(S,S)-dpen}],[15d] contrary to related trans-[RuH$_2${(S)-binap}{tmen}],[15a] was inactive toward hydrogenation. This indicates that the most active reducing agent among all available in solution is the trans-dihydride Ru complex. The origin of this reactivity is due to a trans-effect.[51] Thus, only trans-dihydride Ru complexes were considered.

3. RESULTS AND DISCUSSION

3.1. Enantioselective Reaction of trans-[RuH$_2${(S)-binap}{(S,S)-dpen}] (2) with Acetophenone in Continuum Propan-2-ol: Formation of Ion Pairs and N–H Proton Transfer versus O-Atom Coordination.

The energy profile of the reaction between **2** and acetophenone in continuum propan-2-ol is shown in Figure 1. The reaction starts with the formation of the Re face van der Waals complex **3** formed between **2** and acetophenone. A constrained PES scan along the C$_{acetophenone}$–H–Ru coordinate and subsequent transition state optimization resulted in diastereomeric transition structure **TS$_1$** (i641 cm^{-1}), in which only hydride transfer is taking place as shown in Figures 1 and 2. This process corresponds to a one-bond concerted reaction,[35] because only one bond is broken and formed (Ru–H and C–H), respectively.

Forward IRC calculations from **TS$_1$** led to the identification of **4^{ISIP}**, an inner-sphere[52] ion pair comprised of chiral cationic Ru complex and the (R)-1-phenylethoxide anion as shown in Figure 1 and Supporting Information Figure S4, respectively. The ion pair is additionally stabilized by two noncovalent interactions: strong ionic N–H⋯O$^-$ hydrogen bonding ($d_{N–H}$ = 1.06 Å, $d_{H⋯O}$ = 1.69 Å, d_{NO} = 2.73 Å, N–H–O angle = 165°) and a weak "non-classical" C–H⋯Ru interaction ($d_{C–H}$ = 1.16 Å, $d_{H⋯Ru}$ = 2.13 Å, d_{CRu} = 3.20 Å, C–H–Ru angle = 151°). The weak C–H⋯Ru hydrogen bonding[26,53] preceeds the proton transfer (reverse reaction) during which the hydrogen atom is repolarized. The N–H proton transfer in **4^{ISIP}** via **TS$_2$** (i1069 cm^{-1}) directly yields a hydrogen-bonded adduct of the 16e$^-$ amido complex [RuH{(S)-binap}{(S,S)-HNCHPhCHPhNH$_2$}] with (R)-1-phenylethanol (**5**).

Alternatively, **4^{ISIP}** can yield (R)-1-phenylethoxo complex **6** via dissociation and further O-atom coordination[20,26,28] of the anion. This process is very favorable thermodynamically ($\Delta\Delta G^{\circ}_{298K}$ = −4.8 kcal mol^{-1}; $\Delta\Delta E$ = −8.1 kcal mol^{-1}). Analysis of the PES reveals at least two first-order saddle points lying on the **4^{ISIP}** $\rightarrow$ **6** reaction coordinate. The first saddle-point (i150 cm^{-1}) corresponds to C–H⋯Ru hydrogen-bond cleavage and removal of the C–H bond from Ru ($\Delta\Delta E$ = 0.2 kcal mol^{-1}). The second saddle-point involves O-atom coordination via **TS$_3$**. The very flat nature of the PES in this region prevented its further accurate optimization. This corresponds to a very small activation barrier or even barrierless O-atom coordination. Complex **6** can transform directly into **5** via **TS$_4$** (i849 cm^{-1}), which was computed to be 5.3 kcal mol^{-1} less stable than **TS$_2$** on the free energy scale ($\Delta\Delta G^{\circ}_{298K}$), or 3.6 kcal mol^{-1} on the electronic energy scale ($\Delta\Delta E$).

Inspecting Figure 1, one can conclude that the computations presented in this section adequately describe the stoichiometric experiments of Bergens et al.[11,22] Indeed, complex **6** is the expected kinetic and thermodynamic product of low-temperature reaction between **2** and acetophenone. Upon raising the
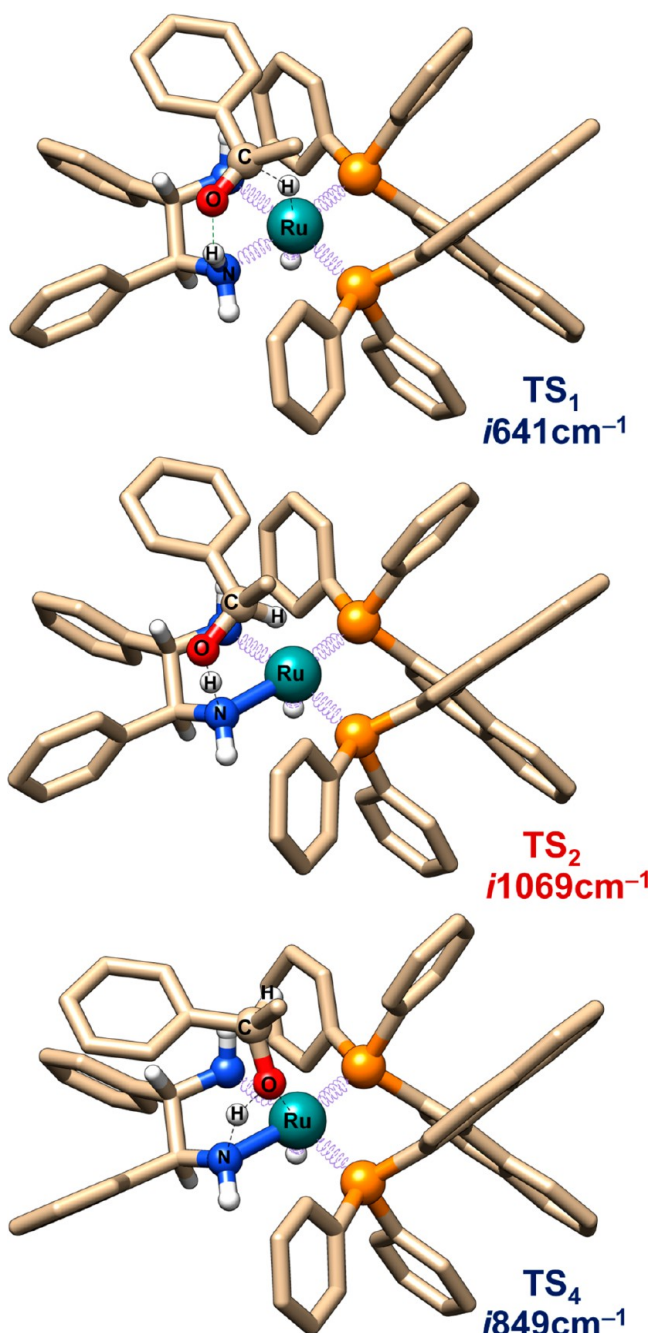
Figure 2. DFT/ωB97X-D/SDD(Ru)/6-31G*(C,H,N,O,P)/SMD-(propan-2-ol)-optimized geometries for transition states **TS$_1$**, **TS$_2$**, and **TS$_4$**. Noncritical hydrogen atoms are removed for the clarity. Green dots correspond to N–H···O$^-$ hydrogen bonding, black dots to the imaginary frequency path.

temperature, equilibrated quantities of H-bonded **5**, "free" (*R*)-1-phenylethanol, and 16e$^-$ amido complex [RuH{(*S*)-binap}-{(*S*,*S*)-HNCHPhCHPhNH$_2$}] should be produced. Whether these products would form directly from **6** or via **4^{ISIP}** would depend on the relative energies of **TS$_2$**, **TS$_3$**, and **TS$_4$**; these may differ with changes in the nature of the catalyst, temperature, solvent, etc. For example, Morris' group has reported that addition of acetophenone to a structurally and electronically modified Noyori catalyst in the form of *trans*-[RuH$_2${(*R*)-binap}{tmen}] (tmen = NH$_2$CH$_2$CH$_2$NH$_2$) in C$_6$D$_6$ (i.e., a low-polarity and noncoordinating solvent) affords

the corresponding 16e$^-$ complex and alcohol.[15b] This is, however, irrelevant to the enantioselectivity (already determined at the earlier stage of the reaction), and the rate of the catalytic reaction (see below).

3.2. H–H Bond Cleavage within Bound Dihydrogen: Three Different Pathways in Continuum Propan-2-ol. The free energy diagram illustrating further transformation of **4^{ISIP}** and regeneration of the catalyst via reaction with H$_2$ is shown in Figure 3. Three different pathways for cleavage of molecular hydrogen as well as three associated transition states are shown in Figures 3 and 4, respectively (**TS$_5$**, **TS$_6$**, and **TS$_7$**).

The most favorable path to release the reaction product from **4^{ISIP}** and regenerate the catalyst follows the blue line in Figure 3. The weak C–H···Ru hydrogen bond[26,53] within **4^{ISIP}** can easily be broken yielding outer-sphere[52] ion pair **4^{OSIP}** as shown in Figure 3 and Supporting Information Figure S4, respectively. The PES of **4^{OSIP}** exhibits different stationary points. An example of such a stationary point is shown in Supporting Information Figure S4 ($\Delta\Delta E$ = 5.6 kcal mol^{-1}).[54] The (*R*)-1-phenylethoxide anion is also bonded to the Ru-cation via an ionic N–H···O$^-$ hydrogen-bonding interaction (d_{N-H} = 1.07 Å, $d_{H···O}$ = 1.67 Å, d_{NO} = 2.68 Å, N–H–O angle = 157°); however, unlike in **4^{ISIP}**, there is a vacant coordination site on the Ru center in **4^{OSIP}**. Binding of molecular hydrogen within the empty coordination site of Ru in **4^{OSIP}** affords hydrogen-bonded ion-pair complex **7**. Two ionic hydrogen bonds stabilize **7**: N–H···O$^-$ (d_{N-H} = 1.04 Å, $d_{H···O}$ = 1.79 Å, d_{NO} = 2.80 Å, N–H–O angle = 163°) and Ru(η^2-H$_2$)···O$^-$ ($d_{O···H}$ = 2.04 Å, d_{ORu} = 3.59 Å, $d_{H–H}$ = 0.81 Å, O–H–Ru angle = 133°). The calculated H–H bond distance of the η^2-H$_2$ ligand in **7** of 0.81 Å suggests a high degree of free H$_2$ character (cf., d_{H-H} = 0.74 Å in an unbound H$_2$ molecule from both theory and experiment[16b]). The lability and high degree of free H$_2$ character of η^2-H$_2$ ligand have been experimentally found for the similar to **7** complex [RuH(η^2-H$_2$){(*R*)-binap}{(*R*,*R*)-dpen}]$^+$BF$_4^-$ at low temperatures.[22c] The following extremely facile deprotonation ($\Delta\Delta G°_{298K}^{\ddagger}$ = 0.4 kcal mol^{-1}; $\Delta\Delta E^{\ddagger}$ = 0.5 kcal mol^{-1}) of the η^2-H$_2$ ligand by (*R*)-1-phenylethoxide anion via **TS$_5$** (*i*330 cm^{-1}) yields the catalyst-product dihydrogen-bonded complex **8**, completing the catalytic cycle.

Dihydrogen bonding (H···H) within **8** preceeds the proton transfer (reverse reaction) to afford an η^2-H$_2$ complex **7**. Such processes are well-documented in the literature.[53,55] This nicely explains the reported[22a] reaction between in situ generated *trans*-[RuH$_2${(*S*)-binap}{(*S*,*S*)-dpen}] with different proton donors to afford alkoxo species in THF-*d$_8$* at −80 °C: dihydrogen evolution occurs from an intermediate dihydrogen complex similar to **7**, not observed by NMR spectroscopy due to its small concentration and lifetime, whereas the alkoxo species similar to **6** are obtained via the ion-pair intermediate **4**. Such a pathway was also proposed by Morris' group, based on NMR experiments with *trans*-[RuH$_2${(*R*)-binap}{tmen}] in C$_6$D$_6$.[15b]

Within this path, complex **7** is a bifurcating point of the reaction and may release the reaction product via four additional pathways (Figure 3). Neutralization of the (*R*)-1-phenylethoxide anion within the ion-pair η^2-H$_2$ Ru complex **7** by solvent via O–H proton transfer[26] (which is equivalent to the replacement of (*R*)-1-phenylethoxide anion within **7** by the isopropoxide anion) affords reaction product (*R*)-1-phenyl-ethanol and the slightly metastable ion-pair η^2-H$_2$ Ru complex **9**. Alternatively, **9** can be obtained by the way of a reversible **7** → **4^{OSIP}** → **4^{ISIP}** → **5** → **9** transformation. In such a scenario,
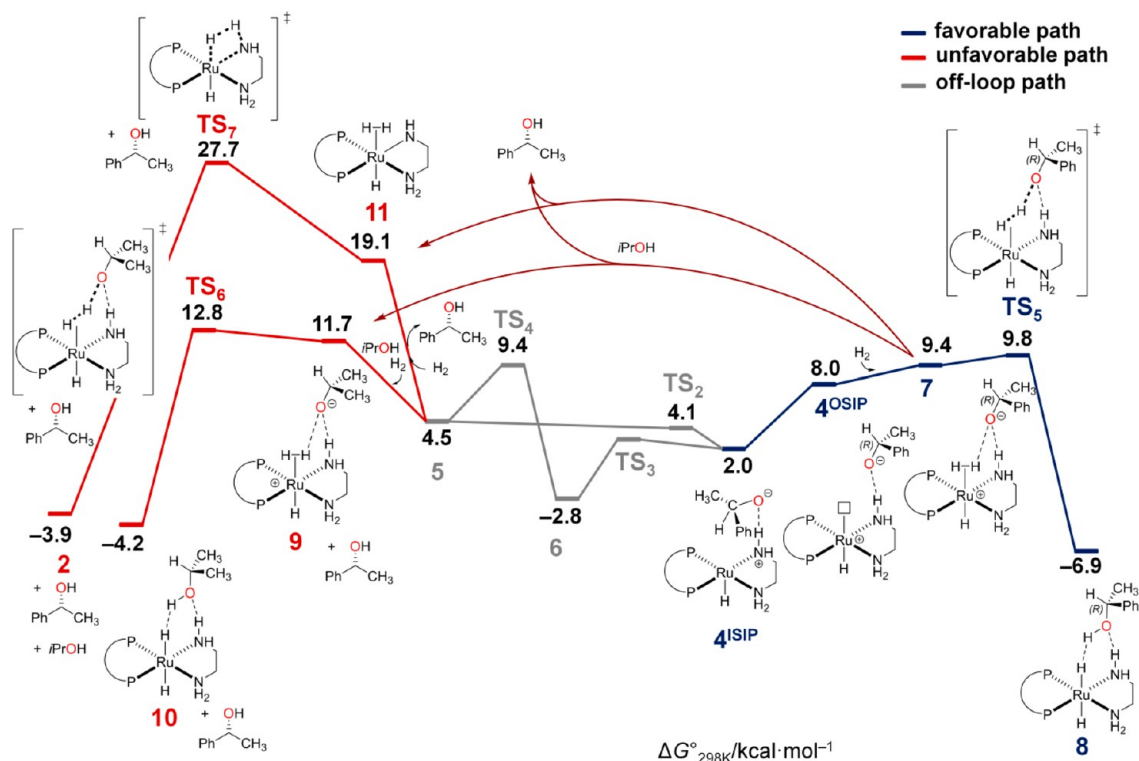
Figure 3. Free energy profile for further transformation of 4^{ISIP} and regeneration of the catalyst via reaction with H_2 computed at DFT/ωB97X-D/SDD(Ru)/6-31G*(C,H,N,O,P)/SMD(propan-2-ol) level of theory. Formation of the major enantiomeric product is shown.

the product is released into solution in the last step of the transformation (step **5** → **9**), and the proton source that neutralizes the (R)-1-phenylethoxide anion in this case is the N–H group of cationic Ru complex 4^{ISIP} occurring during step 4^{ISIP} → **5**. **9** is then obtained via N-protonation of the $16e^-$ amido complex [RuH{(S)-binap}{(S,S)-HNCHPhCHPhNH$_2$}] by solvent following H_2 coordination. The release of the product into solution from **5** and further H_2 coordination would result in neutral metastable η^2-H_2 Ru complex **11** affording the third possibility (**7** → 4^{OSIP} → 4^{ISIP} → **5** → **11**). Finally, N–H proton transfer within cationic η^2-H_2 Ru complex 7^{20} itself may release (R)-1-phenylethanol into solution and would directly afford **11**. In all of these cases, product release into solution is accompanied by metastable intermediates **9** and **11**. The significant instability of neutral η^2-H_2 Ru complex **11** relative to both ion-pair η^2-H_2 Ru complexes **7** and **9**, in which molecular hydrogen is coordinated on the cationic organometallic fragment additionally stabilized by the anion via two ionic hydrogen bonds, is consistent with weaker binding of molecular hydrogen on neutral $16e^-$ complexes relative to cationic derivatives.[59,99] On the other hand, ion-pair η^2-H_2 Ru complex **9** is computed to be 2.3 kcal mol^{-1} less stable than ion-pair η^2-H_2 Ru complex **7** on a free energy scale ($\Delta\Delta G^\circ_{298K}$), or 4.3 kcal mol^{-1} on an electronic energy scale ($\Delta\Delta E$). If single point SDD+f(Ru)/6-311++G**-(C,H,N,O,P)//SDD(Ru)/6-31G*(C,H,N,O,P) calculations are considered, this energy difference is still significant: $\Delta\Delta E$ = 6.2 kcal mol^{-1}. The thermodynamically unfavorable reaction **7** + propan-2-ol = **9** + (R)-1-phenylethanol parallels the reaction (R)-1-phenylethoxide anion + propan-2-ol = (R)-1-phenylethanol + isopropoxide anion and is, probably, due to a higher acidity of (R)-1-phenylethanol versus propan-2-ol.[56]

Regeneration of catalyst **2** from **9** proceeds by a slightly higher energy pathway versus **7**. Our computations predict a slightly higher activation energy versus TS_5 for dihydrogen splitting via TS_6 ($i386$ cm^{-1})[57] in this case ($\Delta\Delta G^\circ_{298K}{}^\ddagger$ = 3.0 kcal mol^{-1}; $\Delta\Delta E^\ddagger$ = 4.3 kcal mol^{-1}). On the other hand, a subsequent (two-bond) concerted four-membered ring process[35] via TS_7 ($i1321$ cm^{-1}), the third possibility for regenerating catalyst **2** via H–H bond cleavage, is too high in energy ($\Delta G^\circ_{298K}{}^\ddagger$ = 27.7 kcal mol^{-1}).[58] In fact, **9** is already computed to be 1.9 kcal mol^{-1}, whereas **11** is 9.3 kcal mol^{-1} less stable than TS_5 (ΔG°_{298K}), a transition state that directly completes the catalytic cycle according to the blue line in Figure 3. Thus, **11** and **9** are not intermediates within the catalytic cycle according to our calculations. However, the slightly higher computed energy of **9** and TS_6 relative to **7** and TS_5, respectively, suggests that **9**, similarly to **5** and **6**, which are true off-loop species, could exist in thermal equilibrium with intermediates of the catalytic cycle, but do not participate in the lowest-energy pathway. Nevertheless, some very small portion of the reaction may proceed via TS_6. It has been reported that partial deuteration (4%) of the reaction product is observed when the reaction is carried out in propan-2-ol-d_8.[7] The origin of this partial deuteration could be due to deutero exchange of coordinated η^2-H_2 ligand with the solvent[59] to afford an η^2-HD ligand within Ru complex **7**. This exchange likely proceeds via the metastable complex **9** and associated TS_6. The higher energy of heterolytic H–H bond cleavage via TS_6 (vs TS_5) is consistent with only partial deuteration of the final product, although the overall interpretation of deuteron exchange seems to be more complex. H–D exchange between propan-2-ol-d_8 and the η^2-H_2 ligand has been experimentally observed for the complex [RuH(η^2-H_2){(R)-binap}{(R,R)-dpen}]$^+$BF$_4^-$ at low temperatures.[22c]

3511

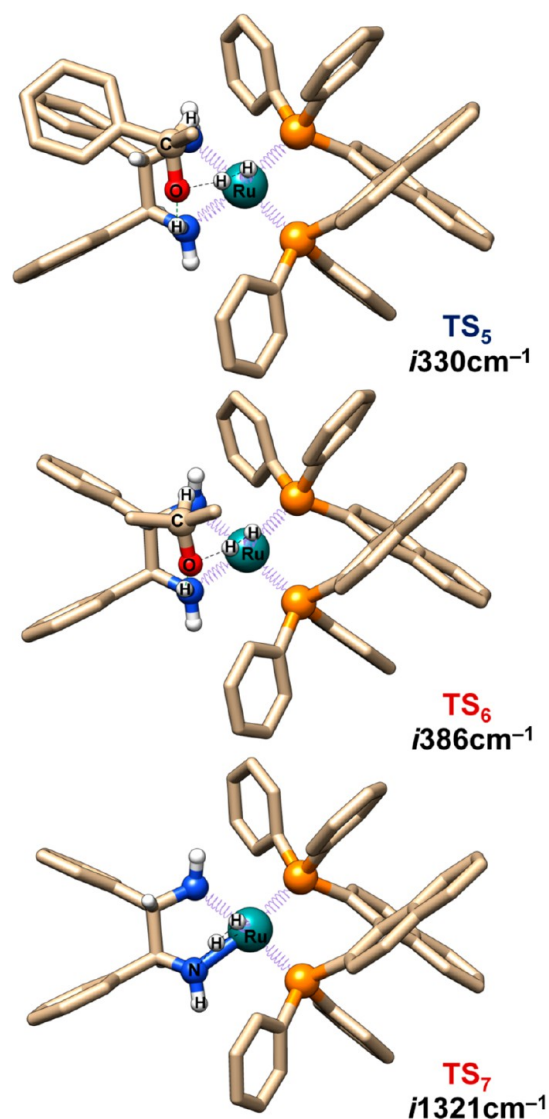dx.doi.org/10.1021/ja411374j | *J. Am. Chem. Soc.* 2014, 136, 3505−3521

Figure 4. H−H bond cleavage: DFT/ωB97X-D/SDD(Ru)/6-31G*-(C,H,N,O,P)/SMD(propan-2-ol)-optimized geometries of the transition states **TS₅**, **TS₆**, and **TS₇**. Noncritical hydrogen atoms are removed for the clarity. Green dots correspond to N−H···O⁻ hydrogen bonding, black dots to the imaginary frequency path.

The 18e⁻ Ru alkoxo complex trans-[RuH{(R)-OCH(CH₃)-(C₆H₅)}{(S)-binap}{(S,S)-dpen}] (**6**) appears to be an "off-cycle" resting state under base-free conditions. For example, the reaction of **6** with propan-2-ol to afford trans-[RuH{OCH-(CH₃)₂}{(S)-binap}{(S,S)-dpen}] and (R)-1-phenylethanol is thermodynamically unfavorable ($\Delta\Delta G_{298K}° = 5.1$ kcal mol⁻¹; $\Delta\Delta E = 7.5$ kcal mol⁻¹).

3.3. Formation of Potassium Amidato Complexes. Hartmann and Chen experimentally demonstrated that, although a base is required for dehydrohalogenation of **2**, the presence of alkoxide ion alone was insufficient for high activity; an alkali metal cation is also necessary.[12] They proposed the formation of alkali amidato complexes of Ru that "participate in rate-limiting states". Recently, the first experimental evidence for such complexes was presented.[60] For the present catalytic system, the effect of the nature of the alkali atom with respect to catalytic activity in propan-2-ol was found to be K > Na ≈ Rb > Li.[12] This order is remarkably similar to that established by Dougherty in water for the strength of metal cation−π

interactions (K > Rb > Na ≈ Li) in contrast to the classical gas-phase electrostatic series Li > Na > K > Rb.[61] This is also qualitatively the same sequence seen in K⁺-selective channels.[62] Several catalytic processes are known to be highly dependent on the presence of alkali metal cations. Among them are aqueous hydrogenations with Wilkinson's catalyst,[63] hydro-genations[64] and transfer hydrogenations of ketones,[65] stereo-selective syntheses,[66] enzymatic reactions,[67] and others.[68] The nature of cation−π interactions was identified as an important factor in molecular recognition in some of these processes.[69] A survey of recent literature data describing the catalytic hydrogenation of carbonyl groups by bifunctional molecular complexes also reveals that medium to high (excess) concentrations of inorganic base such as KO-t-C₄H₉ or EtONa relative to catalyst concentration are always present in the mixture; however, the reasons for reaction acceleration are rather unclear and usually not commented on. Examples that illustrate the need for excess base include commercially available Takasago's complex [RuHCl(dpa)(CO)][28,70] and Gusev's Ru−PNN[71] and Ru−SNS[72] complexes that catalyze more challenging ester hydrogenations,[73] and others for ketone hydrogenations.[17f,74]

We have optimized geometries and compared relative energies of neutral mono- and disubstituted potassium amidato complexes that can be obtained from Noyori's catalyst **2** by reaction with KO-t-C₄H₉ (Supporting Information Figure S5, complexes **2−Kᵃˣ**, **2−Kᵉ𝑞** and **2−Kᵉ𝑞Kᵉ𝑞**, **2−KᵃˣKᵉ𝑞**, **2−KᵃˣKᵃˣ**, respectively). The computed differences in stabilities of various mono- and disubstituted complexes of **2** are typically within −1 to 5 kcal mol⁻¹ relative to **2** and KO-t-C₄H₉/HO-t-C₄H₉. The formation of monosubstituted complexes was computed to be more favorable than the formation of disubstituted complexes. The double deprotonation of two hydrogen atoms attached to the same nitrogen atom is much more unfavorable. An example of a stationary point ($\Delta G_{298K}° = 35.2$ kcal mol⁻¹) is presented in Supporting Information Figure S6. The complexes with potassium in an equatorial position relative to the five-membered NN ring were found to be uniformly more stable than those with axial potassium atom(s). Experimentally, only a monosubstituted potassium amidato complex was observed with an equatorial arrangement of the N−K group in THF-d₈ (**2−Kᵉ𝑞** in Supporting Information Figure S5).[60] Hence, our calculations, although in continuum propan-2-ol, correctly predict the stability of **2−Kᵉ𝑞**. The calculated N−K bond length of 2.70 Å in **2−Kᵉ𝑞** is comparable with experimentally determined in the solid state (X-ray) N−K bond lengths of 2.787(3) Å in [KN(SiMe₃)₂],[75] 2.70(2) Å in [KN(SiMe₃)₂]·2C₄H₈O₂,[76] or other complexes,[77] respectively.

Replacement of N−H hydrogen atoms by potassium within Noyori's catalyst undoubtedly changes the electron density distribution and the nature of the 3D cavity in such a system. In addition to the π−π stacking interaction within the coordinated binap ligand, this is achieved primarily via cation−π interactions[78] involving the phenyl substituents of both dpen and binap ligands. Thus, the relative activation barriers within the catalytic cycle for asymmetric hydrogenation are also expected to be different than in the case of **2**. The computational screening for different neutral mono- and disubstituted potassium amidato complexes reveals that the relative activation barrier for the enantiodetermining hydride transfer appears to decrease by ~1−2 kcal mol⁻¹ (Supporting Information Figure S7). On the other hand, the relative activation barrier for H−H cleavage is much more significantly

reduced (by ~10 kcal mol^{-1}), such that the enantiodetermining hydride transfer now clearly becomes a limiting state (TOF-determining transition state) within the catalytic cycle (Supporting Information Figure S8). Three of the most stable found transition state structures corresponding to hydride transfer and H−H bond cleavage are shown in Figure 5.
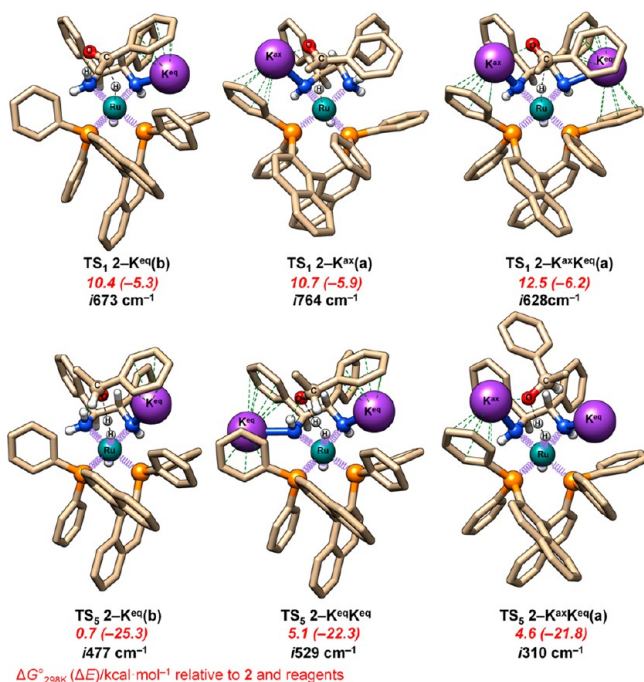

Figure 5. Potassium amidato complexes: DFT/ωB97X-D/SDD(Ru)/6-31G*(C,H,N,O,P,K)/SMD(propan-2-ol)-optimized geometries for three of the most stable found transition state structures corresponding to enantiodetermining hydride transfer (upper), and H−H bond cleavage (below). Noncritical hydrogen atoms are removed for clarity. Green dots correspond to noncovalent interactions (H-bonding, K···O$^-$, or cation−π; π−π stacking are not shown), black dots to the imaginary frequency.

The relative position of saddle points corresponding to hydride transfer and H−H bond cleavage does not necessarily correlate with the calculated position of various stationary points corresponding to potassium amidato complexes with the same structural arrangement on a PES (cf., Supporting Information Figure S5). For example, whereas $2-\mathbf{K^{eq}}$ is the most thermodynamically stable potassium amidato complex from both experiment[60] and theory, enantiodetermining hydride transfer and resulting H−H bond cleavage (via deprotonation of the η^2-H$_2$ ligand by (R)-1-phenylethoxide) indeed occur easily via $\mathbf{TS_1}$ $2-\mathbf{K^{eq}(b)}$ and $\mathbf{TS_5}$ $2-\mathbf{K^{eq}(b)}$, respectively. In all of these structures, potassium occupies the equatorial position within the $\{(S,S)\text{-N(K)H(CHPh)}_2\text{NH}_2\}$ ligand. In the case of the significantly more unstable diamidato $2-\mathbf{K^{ax}K^{eq}}$ ($\Delta\Delta G^\circ_{298K}$ = 6.4 kcal mol^{-1}; $\Delta\Delta E$ = 5.9 kcal mol^{-1} relative to $2-\mathbf{K^{eq}}$), almost equal in energy enantiodetermining hydride transfer via $\mathbf{TS_1}$ $2-\mathbf{K^{ax}K^{eq}(a)}$ takes place.

Relative free energy profiles (FEPs) of active intermediates comprising a plausible simplified catalytic cycle are compared for the classical Noyori's catalyst complex **2** and its potassium amidato derivative $2-\mathbf{K^{eq}}$ in Figure 6.

In each case, only four intermediates comprise the cycle: **2**, $\mathbf{4^{ISIP}}$, **7**, and catalyst-product dihydrogen-bonded complex **8** for the classical Noyori catalyst complex case, as well as $2-\mathbf{K^{eq}}$, $\mathbf{4^{ISIP}}-\mathbf{K^{eq}(b)}$, $\mathbf{7}-\mathbf{K^{eq}(b)}$, and catalyst-product dihydrogen-bonded complex $\mathbf{8}-\mathbf{K^{eq}}$ for the corresponding amidato complex case. Enantiodetermining hydride transfer occurs via $\mathbf{TS_1}$ or $\mathbf{TS_1}$ $2-\mathbf{K^{eq}(b)}$, respectively, whereas dihydrogen bond cleavage occurs via $\mathbf{TS_5}$ or $\mathbf{TS_5}$ $2-\mathbf{K^{eq}(b)}$, respectively. The catalyst-product dihydrogen-bonded complexes **8** and $\mathbf{8}-\mathbf{K^{eq}}$ are not shown in this figure for the sake of clarity. It is assumed that liberation of the product from $\mathbf{TS_5}$ or $\mathbf{TS_5}$ $2-\mathbf{K^{eq}(b)}$ proceeds via **8** and $\mathbf{8}-\mathbf{K^{eq}}$, respectively. Once turnover is completed, the catalyst restarts the cycle at the point below the original one by the reaction energy $\Delta G^\circ_{298K r}$ = −3.88 kcal mol^{-1}. In the case of the cycle involving potassium monoamidato derivative $2-\mathbf{K^{eq}}$, **2** reacts in the first step with KO-t-C$_4$H$_9$ to afford derivative $2-\mathbf{K^{eq}}$ and HO-t-C$_4$H$_9$, respectively. In the last step, $2-\mathbf{K^{eq}}$ is transformed back into **2**. In fact, $2-\mathbf{K^{eq}}$ is very close in energy to complex **2** according
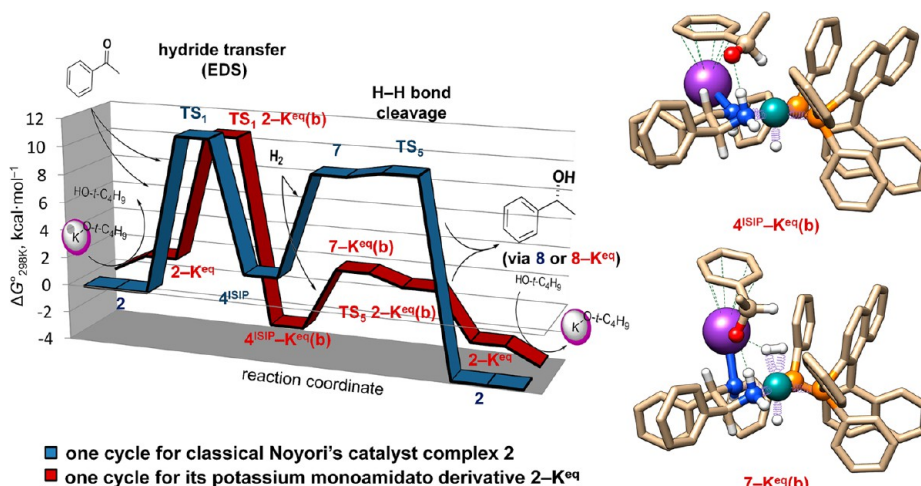

Figure 6. Relative free energy profiles (FEPs) of active intermediates comprising a plausible catalytic cycle for acetophenone hydrogenation are compared for the classical Noyori's catalyst complex **2** and its potassium monoamidato derivative $2-\mathbf{K^{eq}}$ computed at DFT/ωB97X-D/SDD(Ru)/6-31G*(C,H,N,O,P,K)/SMD(propan-2-ol) level of theory. Energy is calibrated relative to complex **2** at the starting and ending points of the cycle. For the optimized geometries of ion pairs $\mathbf{4^{ISIP}}-\mathbf{K^{eq}(b)}$ and $\mathbf{7}-\mathbf{K^{eq}(b)}$, noncritical hydrogen atoms are removed for clarity.

to our calculations ($\Delta\Delta G°_{298K}$ = 1.2 kcal mol^{-1}; $\Delta\Delta E$ = −0.6 kcal mol^{-1}). The optimized geometries of ion pairs 4^{ISIP}−$K^{eq}(b)$ and 7−$K^{eq}(b)$ are also shown in Figure 6 for convenience. In contrast to the case of classical 4^{ISIP}, the 16e$^-$ ion pair complex 4^{ISIP}−$K^{eq}(b)$ is additionally stabilized by at least two K−π interactions.[79] Similarly, the 18e$^-$ ion pair complex 7−$K^{eq}(b)$ is additionally stabilized by one K−π interaction involving N−K^{eq} of the cationic Ru complex and the aromatic ring of the (R)-1-phenylethoxide anion. Moreover, contrary to 7, one additional ionic N−K⋯O$^-$ interaction is present in 7−$K^{eq}(b)$. Interestingly, the angle H^{ax}−N−K^{eq} of 131° in 7−$K^{eq}(b)$ is significantly wider than the corresponding angle of 91° in 4^{ISIP}−$K^{eq}(b)$, possibly due to the structural arrangement of these complexes. The H−H bond length of 0.82 Å in 7−$K^{eq}(b)$ thus places the complex in the category of "true H$_2$ complexes".[59,99] The acidity of such η^2-H$_2$ compounds is sometimes as strong as that of sulphuric or triflic acid.[59,99] The cleavage of the H−H bond in 7−$K^{eq}(b)$ proceeding via TS_5 2−$K^{eq}(b)$ is extremely facile ($\Delta\Delta E^{\ddagger}$ = 0.6 kcal mol^{-1}).

The reversible formation of neutral potassium amidato complexes obtained from 2 by the reaction with KO-t-C$_4$H$_9$ nicely explains the accelerative effect of a large excess of added base. This condition is required to shift the equilibrium from 2 toward the formation of potassium amidato complexes that reduce the relative activation barrier (i.e., relative position of the transition state on PES) of H−H bond cleavage, Figure 6.[80] For example, TS_5 2−$K^{eq}(b)$ is located −10.7 kcal mol^{-1} ($\Delta\Delta E$) or −9.1 kcal mol^{-1} ($\Delta\Delta G°_{298K}$) below TS_5, a main transition state that cleaves molecular hydrogen under KO-t-C$_4$H$_9$-free conditions. If single point SDD+f(Ru)/6-311++G**-(C,H,N,O,P,K)//SDD(Ru)/6-31G*(C,H,N,O,P,K) calculations are considered, this energy difference is still significantly high: $\Delta\Delta E$ = −5.0 kcal mol^{-1}. Thus, a possible factor that stabilizes TS_5 2−$K^{eq}(b)$ versus TS_5 seems to be the presence of cation−π interaction. Of note, many studies have shown that cation−π interactions enhance binding energies by 2−5 kcal mol^{-1}.[69a] The accelerated cleavage of hydrogen via the measured increased relative rate of H$_2$ consumption in the presence of KO-t-C$_4$H$_9$ was directly observed in kinetics curves.[12]

The substitution of N−H hydrogen atom(s) with potassium within Noyori's catalyst 2 may not only reduce the symmetry, but also increase the number of isomers participating in the reaction. In Figure 6, only the path proceeding via 2−K^{eq} is shown. However, when amidato complexes are involved, enantiodetermining hydride transfer may occur equally on different mono- and diamidato complexes as discussed above. Examples of these almost equal in energy transition states leading to (R)-1-phenylethanol are shown in Figure 5. On the other hand, however, it seems that dihydrogen cleavage proceeds via TS_5 2−$K^{eq}(b)$, based on the present calculations.

3.4. Rate-Determining Transition Structure and KIE.
Assuming that hydride transfer is a rate-determining state, the composition of the enantiomers (% ee) would be determined by the free energy difference between two diastereomeric transition states leading to opposite enantiomer formation (for discussion on enantioselectivity, see below). Our calculations do not provide qualitative information on the nature of the rate-determining state under base-free conditions as the computed energies of TS_1 ($\Delta G°_{298K}$ = 11.3 kcal mol^{-1} vs 2) and TS_5 ($\Delta G°_{298K}$ = 9.8 kcal mol^{-1} vs 2) are within the errors of the DFT methodology used (Figure 6).[81] If TS_5 is a rate-determining step, the composition of the enantiomers (% ee)

would be determined by the free energy difference between the two diastereomeric transition states only under the assumption that the preceding hydride transfer is an irreversible step. Experimentally the reaction with H$_2$/(CH$_3$)$_2$CHOH proceeds 50 times faster than that with D$_2$/(CD$_3$)$_2$CDOD in the absence of base.[7] The significantly high value of KIE* = 50, which combines kinetic (KIEs) and kinetic solvent[82] isotope effects (KSIEs), may serve as evidence that H−H bond cleavage is involved in the rate-determining state (or, at least, in one of the states affecting the reaction rate) or perhaps evidence of significant proton tunneling.[83] The calculated values for the KIE of single step for transformations $3 \to TS_1$ (k_H/k_D = KIE = 1.64) and $7 \to TS_5$ (k_{HH}/k_{DD} = KIE = 1.62) and the fact the reaction still proceeds at lower temperatures[11,22b] suggest that proton tunneling may occur.

Under high KO-t-C$_4$H$_9$ concentrations, the transition state corresponding to hydride transfer is clearly rate-determining (or TOF-determining); see Figure 6. Under these conditions, the reaction may be assumed to follow an energetic span approximation,[48] a model that is derived with three conditions: (i) transition state theory (TST) is valid, (ii) a steady-state regime is applicable, and (iii) the intermediates undergo fast relaxation. The TOF-determining transition state (also enantiodetermining) is hydride transfer (transition states TS_1 2−$K^{eq}(b)$ or TS_1 2−$K^{ax}(a)$, Figure 5), whereas the TOF-determining intermediate seems to be a Ru alkoxo mono-amidato complex (Supporting Information Figure S10, 6−K^{ax}).[84] The energetic span (δE) calculated as $\Delta\Delta G_{298K}°_{cycle}$ = $\Delta G_{298K}°(TS_1$ 2−$K^{eq}(b)) - \Delta G_{298K}°(6$−$K^{ax}) + \Delta G_{298K}°_r$ = 10.44 − (−6.57) + (−3.88) = 13.13 kcal mol^{-1} allows us to estimate the TOF of the reaction under standard conditions[91] and in basic media as 1476 s^{-1}. For TS_1 2−$K^{ax}(a)$, this value becomes $\Delta G_{298K}°_{cycle}$ = 13.43 kcal mol^{-1}, which gives TOF of 889 s^{-1}. Both values could be compared to the experimentally determined initial TOF of 583 s^{-1} for $1e$ after 2−3 min,[3] or TOF of 63 s^{-1} for $1b$ at 30% conversion and 30 °C ($\Delta\Delta G_{303K}°_{cycle,calcd}$ = 15.27 kcal mol^{-1}).[1e] The nearly quantitative agreement is no doubt fortuitous,[85] but one can compare that with the presently accepted mechanism under conditions of high base concentration (Scheme 1, catalytic cycle II). Here, the rate-determining transition state is H−H bond cleavage via $TS_2(a)$,[7,13] and the energetic span (δE) should be calculated[48] as $\Delta\Delta G_{298K}°_{cycle}$ = $\Delta G_{298K}°(TS_7) - \Delta G_{298K}°(6)$ = 27.69 − (−2.80) = 30.49 kcal mol^{-1}, which gives an extremely small TOF of 2.78 × 10^{-10} s^{-1}. This is 11−12 orders of magnitude different from the experimentally observed values. For multibond concerted $TS_2(b)$ (the analogue of which in continuum solvent is the one-bond concerted TS_6 in Figure 3), the $\Delta\Delta G_{298K}°_{cycle}$ = $\Delta G_{298K}°(TS_6) - \Delta G_{298K}°(6)$ = 12.83 − (−2.80) = 15.63 kcal mol^{-1}, which gives a TOF of 22 s^{-1}. This is still feasible,[85] and some portion of the reaction may occur via this pathway.

In the presence of base, the reaction with H$_2$/(CH$_3$)$_2$CHOH proceeds 2 times faster than with D$_2$/(CD$_3$)$_2$CDOD.[7] Calculation of the energetic span (δE^D) for the selectively deuterated species along the reaction coordinate as $\Delta\Delta G_{298K}°_{cycle}{}^D$ = $\Delta G_{298K}°(TS_1$ 2−$K^{ax}(a)^D) - \Delta G_{298K}°(6$−$K^{axD}) + \Delta G_{298K}°_r{}^D$ = 18.49 + (−5.50) = 12.99 kcal mol^{-1} allows us to calculate the kinetic isotope effect of the entire catalytic reaction based on TST formula[86] as KIE = 0.79.[87] The discrepancy between this calculated value and experiment (KIE* = 2) is somewhat unsettling, as isotope effects computed for simple reactions (steps), as opposed to the entire cycle as

Table 1. Energy Difference between *S*- and *R*-Enantioselective Pathways Taking Place on Complexes 2, 2−K^{ax}(a), and 2−K^{ax}K^{eq}(a) as well as Calculated Enantioselectivity

reactive complex	$\Delta\Delta E$, kcal mol^{-1}	calcd ee, %	$\Delta\Delta E_{ZPVE}$, kcal mol^{-1}	calcd ee, %	$\Delta\Delta G_{298K}°$, kcal mol^{-1}	calcd ee, %
2	2.43	96.960	3.37	99.387	3.55	99.550
2−K^{ax}(a)	3.81	99.712	3.79	99.702	2.35	96.521
2−K^{ax}K^{eq}(a)	6.24	99.996	6.04	99.994	4.88	99.954

we have done here, are usually reasonably accurate.[88] A potential source of error may come from inaccurate calculations of the entropy changes by DFT.[89] The divergence may also be a result of the different physical nature of (CH$_3$)$_2$CHOH versus (CD$_3$)$_2$CDOD because the observed KIE* also includes a KSIE contribution. Isotopic substitution somewhat changes the dielectric and HBD (hydrogen-bond donor)/HBA (hydrogen-bond acceptor)[34] properties of solvents, which in turn can change the reorganization energy.[83c] This has a direct influence on the observed reaction rate through dynamic or frictional effects.[34] Finally, the discrepancy may also arise from our use of the energetic span approximation itself. It is interesting to note in this context that the KIE for the rate-determining hydride transfer reaction itself is 1.80 (model 3−K^{ax}(a) → TS$_1$ 2−K^{ax}(a)), in close agreement with the experimental KIE*. We report computed KIEs for all individual steps in the Supporting Information.

3.5. Enantioselectivity. It is important to understand the factors governing the enantioselectivity within the newly established mechanism. In this work, we have shown that enantioselection takes place when hydride transfer occurs and the chiral anion is formed (i.e., TS$_1$, TS$_1$ 2−K^{eq}(b), TS$_1$ 2−K^{ax}(a), TS$_1$ 2−K^{ax}K^{eq}(a), etc.). The enantioselective stage has been evaluated using classical Noyori's catalyst complex 2 as well as mono- and diamidato complexes 2−K^{ax}(a) and 2−K^{ax}K^{eq}(a), respectively. Monoamidato complex 2−K^{ax}(a) has been particularly chosen as a reactive center because the H/K substitution here involves the axial NH proton, which was considered to participate in the putative six-membered pericyclic transition state, initially giving rise to the term "metal−ligand bifunctional mechanism".[10] The "opposite" scenarios to diastereomeric transition states TS$_1$, TS$_1$ 2−K^{ax}(a), and TS$_1$ 2−K^{ax}K^{eq}(a), which lead to (*S*)-1-phenylethanol production, are shown in Supporting Information Figure S11 (TS$_1$^{opp}, TS$_1$ 2−K^{ax}(a)^{opp}, and TS$_1$ 2−K^{ax}K^{eq}(a)^{opp}, respectively). The energy difference[90] between *S*- and *R*-enantioselective pathways as well as calculated enantioselectivity is summarized in Table 1.

In all of the studied cases, both sense and order of enantioselection are well reproduced. For the classical Noyori's complex 2, the energy differences between TS$_1$^{opp} and TS$_1$ of 2.43 ($\Delta\Delta E$), 3.37 ($\Delta\Delta E_{ZPVE}$), and 3.55 kcal mol^{-1} ($\Delta\Delta G_{298K}°$) are comparable with the experimentally observed enantioselectivity (80−97% ee,[1a] 1.27−2.43 kcal mol^{-1}).[91] The key factor that destabilizes TS$_1$^{opp} is the repulsive interaction between the acetophenone aromatic ring and a portion of the binap ligand (phenyl substituent and one aromatic ring of naphthalene). Thus, destabilization of TS$_1$^{opp} is achieved primarily due to steric factors. Any increase in the bulkiness of the phenyl substituent of the binap ligand is expected to destabilize TS$_1$^{opp} to a greater extent. This is indeed the case: (*S*)-XylBINAP/(*S*,*S*)-DPEN ruthenium complexes yielded better enantioselectivities than (*S*)-BINAP/(*S*,*S*)-DPEN or (*S*)-TolBINAP/(*S*,*S*)-DPEN combinations.[5b] On the other hand, for TS$_1$ there are no steric repulsions. The weak N−H···π hydrogen bonding

between one N−H moiety and the π-density of an aromatic ring of acetophenone initially formulated[92] as the origin of the enantioselectivity is rather viewed here as a "forced" interaction, which does not seem to stabilize TS$_1$ in a significant way, according to our models. The N−H proton is not orientated toward the center of the aromatic ring, but instead toward two carbon atoms (2.44 and 2.63 Å, respectively, see Cartesian Coordinates in the Supporting Information). Thus, the absence of any steric repulsion appears to be the main factor contributing to the relative stability of TS$_1$.

For the mono- and diamidato complexes 2−K^{ax}(a) and 2−K^{ax}K^{eq}(a), the energy difference for each couple [TS$_1$ 2−K^{ax}(a)]/[TS$_1$ 2−K^{ax}(a)^{opp}] and [TS$_1$ 2−K^{ax}K^{eq}(a)]/[TS$_1$ 2−K^{ax}K^{eq}(a)^{opp}] increases proportionally to the number of K-atoms present: 3.81 and 6.24 kcal mol^{-1} ($\Delta\Delta E$), respectively. This is achieved primarily via the more organized (rigid) structure of the complexes, as a result of cation−π interactions. The key stabilizing/destabilizing factors are similar to the case of [TS$_1$]/[TS$_1$^{opp}]. The difference as compared to classical complex 2 is the presence of cation−π interactions (i.e., acetophenone···K) as a stabilizing factor within the major pathway (see, for example, TS$_1$ 2−K^{ax}K^{eq}(a)). It appears that replacement of N−H hydrogen atoms with potassium within Noyori's catalyst may increase the enantioselectivity via the higher energy difference of the corresponding diastereomeric transition states. This trend is observed for the couples [TS$_1$ 2−K^{ax}(a)]/[TS$_1$ 2−K^{ax}(a)^{opp}] and [TS$_1$ 2−K^{ax}K^{eq}(a)]/[TS$_1$ 2−K^{ax}K^{eq}(a)^{opp}], relative to the classic [TS$_1$]/[TS$_1$^{opp}]. The reaction coordinate leading to (*S*)-1-phenylethanol likely proceeds through only one, most stable first-order saddle point, or through several first-order saddle points having similar or very close energies on the PES. For example, the computed energy difference between TS$_1$ 2−K^{ax}(a)^{opp} and TS$_1$ 2−K^{ax}K^{eq}(a)^{opp} is only −2.05 kcal mol^{-1} (ΔE), which computationally[85] corresponds to the same energy. Thus, (*S*)-1-phenylethanol could be obtained via both TS$_1$ 2−K^{ax}(a)^{opp} and TS$_1$ 2−K^{ax}K^{eq}(a)^{opp}. In conclusion, *S*- and *R*-enantioselective pathways may take place via different isomers of *trans*-[RuH$_2${(*S*)-binap}{(*S*,*S*)-N(K)H(CHPh)$_2$NH$_2$}] or *trans*-[RuH$_2${(*S*)-binap}{(*S*,*S*)-N(K)H(CHPh)$_2$NH(K)}]. On the basis of the most stable transition states found in this work, when high KO-*t*-C$_4$H$_9$ excess is present, (*R*)-1-phenylethanol formation proceeds almost equally via TS$_1$ 2−K^{eq}(b), TS$_1$ 2−K^{ax}(a), or TS$_1$ 2−K^{ax}K^{eq}(a), whereas (*S*)-1-phenylethanol formation proceeds via TS$_1$ 2−K^{ax}(a)^{opp} and TS$_1$ 2−K^{ax}K^{eq}(a)^{opp}. For the couple [TS$_1$ 2−K^{ax}(a)]/[TS$_1$ 2−K^{ax}(a)^{opp}], the energy difference is 6.24 ($\Delta\Delta E$), 6.04 ($\Delta\Delta E_{ZPVE}$), and 4.88 kcal mol^{-1} ($\Delta\Delta G_{298K}°$), respectively. The enantioselection is thus slightly higher than for the classic couple TS$_1$/TS$_1$^{opp}.

3.6. Multiple Roles of KO-*t*-C$_4$H$_9$. Evaluation of a Possible Background Reaction Catalyzed by KO-*t*-C$_4$H$_9$. In addition to the formation of neutral potassium amidato complexes, the role of the KO-*t*-C$_4$H$_9$ appears to be several fold in this system.[93,94] In addition to dehydrochlorination[5b] of the
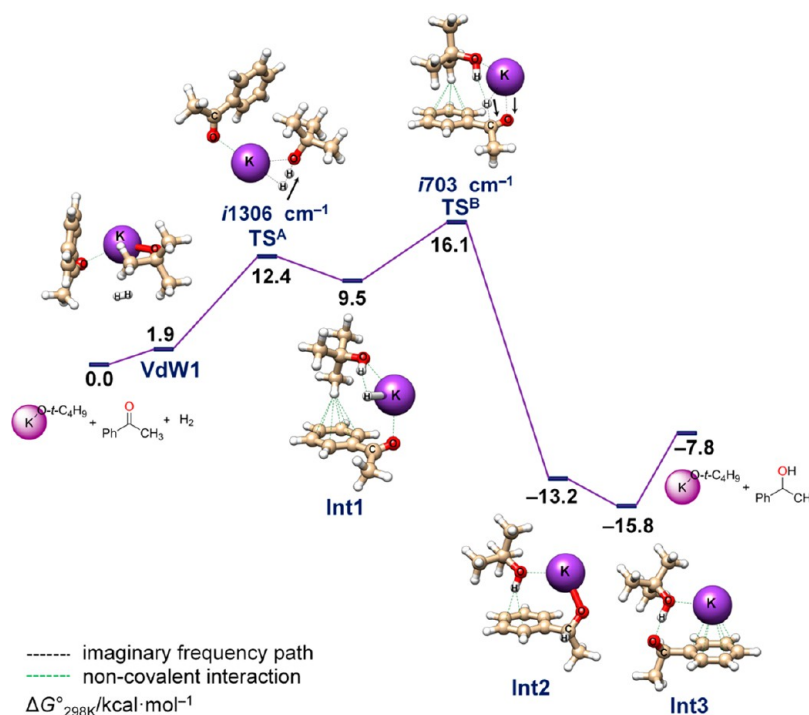
Figure 7. Mechanism of KO-t-C$_4$H$_9$-catalyzed acetophenone hydrogenation computed at DFT/ωB97X-D/6-311++G**(C,H,O,K)/SMD(propan-2-ol) level of theory.
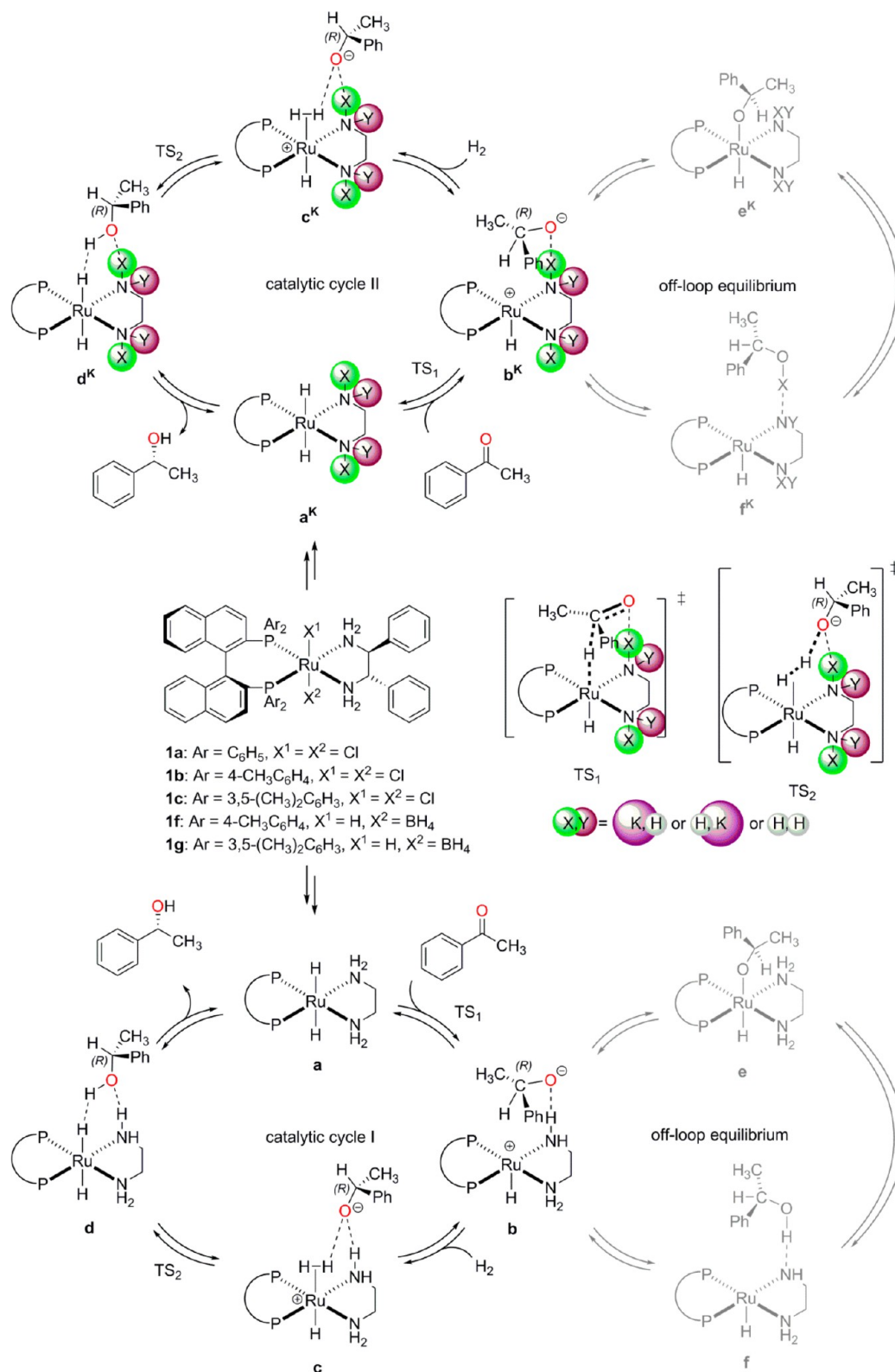
catalyst precursor **1** and possible regeneration of its active form[11] from the alkoxo complex formed during catalysis, there could be effects related to the polarity and coordinative ability of the reaction medium. Because KO-t-C$_4$H$_9$ is a salt, increasing its concentration may increase the ionic strength[95] of a solution, leading to an increase in its polarity.[34] Alkali cation "cocatalysis", that is, when an alkali cation itself could bind to the neutral complex **2** via cation−π interactions, was also proposed as a possibility,[12] although the overall effect seems to be less profound than direct NH/NK substitution described herein.

Finally, a possible (background) ketone hydrogenation reaction catalyzed by KO-t-C$_4$H$_9$ occurring without any enantioselection may decrease the observed enantioselectivity under basic conditions.[96] Berkessel and co-workers demonstrated that almost complete conversions of ketones could be achieved,[96a] albeit under harsh reaction conditions (ca. 200 °C, >100 bar H$_2$, 20 mol % potassium $tert$-butoxide as base) in $tert$-butanol as solvent.[97] A six-membered pericyclic transition state similar to **TS$_1$** in Figure 1 has been proposed, although experimental evidence suggested that H−H bond cleavage is not the rate-determining state.[96a] On the basis of DFT/ωB97X-D/6-311++G**(C,H,O,K)/SMD(propan-2-ol) computations, we found that in solution, the KO-t-C$_4$H$_9$-catalyzed acetophenone hydrogenation represents a two-step reaction,[35] that is, proceeds via kinetically distinct steps as shown in Figure 7. In the first step of the reaction, cleavage of the H−H bond takes place across an O−K bond (transition state: **TS^A**), and a hydrogen-bonded adduct **Int1** is formed. The IRC path also includes van der Waals complex **VdW1**. **Int1** represents an HK molecule bonded to HO-t-C$_4$H$_9$ via two noncovalent interactions (H···H dihydrogen bonding and O···K bonding). At the same time, **Int1** is bonded to acetophenone via O···K bonding. In the second step of the reaction, addition of H−K to C=O of acetophenone occurs via **TS^B**, and this is the state that

is rate-determining. Forward IRC calculations from **TS^B** lead to the identification of **Int2**, which represents potassium phenylethoxide bonded to HO-t-C$_4$H$_9$ via O−H···π hydrogen bonding and O−K···O interaction, respectively. **Int2** is in equilibrium with its isomer **Int3**, in which a potassium cation is bonded to the aromatic ring via cation−π interaction in a similar fashion to cyclopentadienyl-alkalimetal complexes,[98] and rather to oxygen anion. This is the intermediate that is a resting state (or TOF-determining intermediate). Finally, H/K exchange within the HO-t-C$_4$H$_9$/potassium phenylethoxide couple completes turnover. The proton transfer in **Int3** is extremely facile ($\Delta\Delta E^{\ddagger}$ = 0.2 kcal mol^{-1}; for the geometry of the corresponding saddle point **TS^C**, see the Supporting Information). The catalyst restarts the cycle at the point below the original one by the reaction energy $\Delta G_{298K}^{\circ}{}_r$ = −7.75 kcal mol^{-1}. The energetic span (δE) calculated[48] as $\Delta\Delta G_{298K}^{\circ}{}_{cycle}$ = $\Delta G_{298K}^{\circ}(\mathbf{TS^B})$ − $\Delta G_{298K}^{\circ}(\mathbf{Int2})$ + $\Delta G_{298K}^{\circ}{}_r$ = 16.11 − (−15.76) + (−7.75) = 24.12 kcal mol^{-1} allows us to estimate the TOF of the KO-t-C$_4$H$_9$-catalyzed acetophenone hydrogenation under standard conditions[91] as 1.30×10^{-5} s^{-1}. This is 8 orders of magnitude different from the calculated TOF of 1476 s^{-1} for the catalytic cycle in which potassium amidato complexes participate (vide supra). The overall kinetics expressed in TOFs should also include concentration effects.[48] Thus, under high H$_2$ pressures and high KO-t-C$_4$H$_9$/Ru ratios, one should be cognizant of the possible background reaction.

Evaluation of a possible direct KO-t-C$_4$H$_9$-catalyzed contribution to the enantiomeric purity of the final product is problematic, but several available experimental data can be examined and subjected to speculation. For example, when complex **1b** is used with acetophenone/Ru/KO-t-C$_4$H$_9$ = 2 400 000/1/24 000 (45 atm H$_2$, 30 °C for 48 h), (R)-1-phenylethanol is obtained in 100% yield (94% yield after distillation) and with only 80% ee.[1e] The same ee (82%) and yield are obtained, when **1b** is used in form of **1f** under base-

3516

dx.doi.org/10.1021/ja411374j | J. Am. Chem. Soc. 2014, 136, 3505−3521

Scheme 3. A Revised Catalytic Cycle for the Asymmetric Hydrogenation of Acetophenone Catalyzed by an Active Form of 1 (Formation of the Major Enantiomeric Product Is Shown): Catalytic Cycle I (KO-*t*-C$_4$H$_9$-Free Conditions), Catalytic Cycle II (Under High KO-*t*-C$_4$H$_9$ Concentration)

1a: Ar = C$_6$H$_5$, X^1 = X^2 = Cl
1b: Ar = 4-CH$_3$C$_6$H$_4$, X^1 = X^2 = Cl
1c: Ar = 3,5-(CH$_3$)$_2$C$_6$H$_3$, X^1 = X^2 = Cl
1f: Ar = 4-CH$_3$C$_6$H$_4$, X^1 = H, X^2 = BH$_4$
1g: Ar = 3,5-(CH$_3$)$_2$C$_6$H$_3$, X^1 = H, X^2 = BH$_4$

free conditions, acetophenone/Ru = 100 000/1 (8 atm H$_2$, 23–38 °C).[6] Although the observed enantioselectivity is essentially the same, a direct comparison is impossible, because different reaction conditions are applied. If enantioselectivity due to the base-catalyzed reaction is indeed negligible, then the observed enantioselectivity is only due to the intrinsic nature of catalyst **1b**, which should give the same result as **1f**, as observed. Alternatively, in this example that uses high KO-*t*-C$_4$H$_9$

concentration (Ru/KO-t-C$_4$H$_9$ = 1/24 000), catalyst **1b** is structurally modified (catalytic reaction takes place on potassium amidato complexes), and the degree of the enantioselection could be higher as discussed above. The observed 80% ee may be due to "enantiopoisoning" by a possible (nonenantioselective) background contribution from KO-t-C$_4$H$_9$ catalysis. Higher hydrogen pressure (45 atm H$_2$) may also facilitate this reaction.

In fact, hydrogenation of 1′-acetonaphthone by **1b** in the presence of much less base and under reduced H$_2$ pressure (Ru/KO-t-C$_4$H$_9$ = 1/200 at 10 atm H$_2$) yields (R)-1-(1-naphthyl)ethanol in 93% yield and with higher enantioselectivity versus (R)-1-phenylethanol (91% ee).[1e] The comparison is again inexact, because a different ketone is used.

In another example utilizing structurally slightly different catalyst **1c** and acetophenone/Ru/KO-t-C$_4$H$_9$ = 100 000/1/ 400 (8 atm H$_2$, 28 °C), (R)-1-phenylethonol is recovered qualitatively with 99% ee.[1g] The same ee is obtained, when **1c** is used in form of **1g** under base-free conditions, acetophenone/ Ru = 100 000/1 (8 atm H$_2$, 45 °C). Albeit in this case, reaction is complete within 7 h versus 45 min in the presence of the base.[6] In this example, the catalyst is structurally different (a more congested xylbinap ligand is better for enantioselectivity), and the amount of base is significantly lower (Ru/KO-t-C$_4$H$_9$ = 1/400). In this case, any background contribution from KO-t-C$_4$H$_9$-catalyzed hydrogenation is small (if any), and the reaction proceeds with better ee. In conclusion, any single model that describes all catalyst activities is impossible, as a change made to one parameter may impact other multiple factors, not necessarily in the same way and extent.

3.7. Catalytic Cycle. The experimental observation that the reaction with H$_2$/(CH$_3$)$_2$CHOH proceeds 50 times faster than that with D$_2$/(CD$_3$)$_2$CDOD in the absence of base, but the rate differs only by a factor of 2 in the presence of KO-t-C$_4$H$_9$, promoted Noyori and co-workers to propose that dual mechanisms are in operation giving a rise to the two catalytic cycles shown in Figure 1.[7] Our results presented here, as well as analysis of the most recent experimental data, indeed suggest that based on the presence or absence of KO-t-C$_4$H$_9$ a dual mechanism is in operation; however, the current picture is different.

The proposed simplified scenario is shown in Scheme 3. The catalytic cycles without K-substitution (catalytic cycle I: KO-t-C$_4$H$_9$-free conditions) and with K-substitution (catalytic cycle II: in the presence of KO-t-C$_4$H$_9$) are qualitatively similar. Only four active intermediates comprise the cycle, that is, complexes **a** (**a^K**), **b** (**b^K**), **c** (**c^K**), and catalyst-product dihydrogen-bonded complex **d** (**d^K**), respectively. The catalyst coordinates the substrate via noncovalent interactions, and an enantiodetermining hydride transfer via **TS$_1$** takes place. The vacant coordination site formed at Ru is occupied by dihydrogen that promotes its splitting via **TS$_2$**, yielding the reaction product and recovering the catalyst. Complexes **e** (**e^K**) and **f** (**f^K**) exist in thermal equilibrium during the catalytic cycle, but do not directly participate in the lowest-energy pathway. Complex **e** (**e^K**) seems to be the resting state (TOF-determining intermediate) off the catalytic cycle.

Whereas under high base concentration, the rate-determining transition state clearly corresponds to the enantiodetermining hydride transfer (cycle II), our calculations do not provide qualitative information on the nature of this state under base-free conditions, because the computed energy of the transition

states corresponding to hydride transfer and H−H bond cleavage is very close (cycle I).

The sophisticated mechanism of acetophenone or other ketone hydrogenation catalyzed by **1** seems likely to be much more complex. In fact, because the reaction itself is dynamic, even under a fixed set of parameters, it was reported that turnover-limiting states could change with time and extent of turnover from hydride transfer to dihydrogen cleavage or vice versa.[12a] One may speculate that this change could be due to shifts in complex equilibria involving KO-t-C$_4$H$_9$ among other species. Indeed, with extent of turnover, slight acidification seems to occur because the reaction product (R)-1-phenylethanol is more acidic than propan-2-ol.[56] Thus, accumulation of the product may also change equilibria in which KO-t-C$_4$H$_9$ is involved.

4. CONCLUSIONS

A revised mechanism (catalytic cycle) for the hydrogenation of acetophenone by Noyori's catalyst, in the presence or absence of KO-t-C$_4$H$_9$, has been formulated. Analyzing the most recent experimental observations, avoiding gas-phase calculations, and applying full atomistic models optimized in continuum solvent reaction field under DFT/ωB97X-D/SDD(Ru)/6-31G*-(C,H,N,O,P,K)/SMD(propan-2-ol), the reaction appears to proceed via different intermediates and transition states as compared to those previously proposed. For example, the 16e⁻ Ru amido complex [RuH{(S)-binap}{(S,S)-HN-(CHPh)$_2$NH$_2$}] and the 18e⁻ Ru alkoxo complex *trans*-[RuH{OCH(CH$_3$)(R)}{(S)-binap}{(S,S)-dpen}] (R = CH$_3$ or C$_6$H$_5$) are not intermediates within the catalytic cycle, but rather are off-loop species. Theoretical calculations performed in dielectric continuum consistent with experimental data indicate that there does not appear to be any six-membered pericyclic transition state or any multibond concerted ones at play. Hydride transfer (the enantio- and rate-determining step) still proceeds in an outer-sphere manner as originally suggested by Noyori et al.; however, only one bond is cleaved (Ru−H) and formed (C−H), respectively. The presence of ion pairs within the reaction coordinate permits H−H bond cleavage via a simple deprotonation step by the (R)-1-phenylethoxide anion, aided by an electrophilic Ru center. In other words, the η^2-H$_2$ ligand within the cationic Ru complex serves as an acid to neutralize the (R)-1-phenylethoxide anion.[59,99] This appears to be the lowest energy pathway available to cleave molecular H$_2$. A solvent-assisted pathway for cleavage of H$_2$ also seems to be energetically feasible; however, direct H−H bond cleavage on 16e⁻ Ru appears to be too high in energy. The accelerating effect of a large excess of KO-t-C$_4$H$_9$ has also been rationalized computationally. Potassium monosubstituted *trans*-[RuH$_2${(S)-binap}{(S,S)-N(K)H(CHPh)$_2$NH$_2$}] or disubstituted amidato complexes *trans*-[RuH$_2${(S)-binap}{(S,S)-N(K)H-(CHPh)$_2$NH(K)}] reversibly formed via reaction of Noyori's catalyst with KO-t-C$_4$H$_9$ directly participate in the catalytic cycle and lower the relative barriers for hydride transfer and more significantly H−H bond cleavage. The synergism of steric and electronic effects triggered by cation−π interactions seems to be an important factor responsible for the experimentally observed increase in turnover. The results lend credence to and complement the original proposals of Chen et al. based on kinetics studies,[12] as well as recent experimental findings in Bergens' group.[60]

In summary, one may speculate that NH/NK or NH/NNa, etc., substitution as described in this Article and documented

experimentally[12,60] could be an important factor responsible for the acceleration of some hydrogenation reaction rates within the area of bifunctional molecular catalysis.[100]

■ ASSOCIATED CONTENT

ⓈSupporting Information

Cartesian coordinates for all optimized compounds, tables of energy data, summary of KIEs, complete ref 30, examples of input files, and other details. This material is available free of charge via the Internet at http://pubs.acs.org.

■ AUTHOR INFORMATION

Corresponding Authors

pdub@lanl.gov
jgordon@lanl.gov

Notes

The authors declare no competing financial interest.

■ ACKNOWLEDGMENTS

■ REFERENCES

(1) (a) Ohkuma, T.; Ooka, H.; Hashiguchi, S.; Ikariya, T.; Noyori, R. *J. Am. Chem. Soc.* **1995**, *117*, 2675. (b) Ohkuma, T.; Ooka, H.; Ikariya, T.; Noyori, R. *J. Am. Chem. Soc.* **1995**, *117*, 10417. (c) Ohkuma, T.; Ooka, H.; Yamakawa, M.; Ikariya, T.; Noyori, R. *J. Org. Chem.* **1996**, *61*, 4872. (d) Ohkuma, T.; Ikehira, H.; Ikariya, T.; Noyori, R. *Synlett* **1997**, 467. (e) Doucet, H.; Ohkuma, T.; Murata, K.; Yokozawa, T.; Kozawa, M.; Katayama, E.; England, A. F.; Ikariya, T.; Noyori, R. *Angew. Chem., Int. Ed.* **1998**, *37*, 1703. (f) Ohkuma, T.; Doucet, H.; Pham, T.; Mikami, K.; Korenaga, T.; Terada, M.; Noyori, R. *J. Am. Chem. Soc.* **1998**, *120*, 1086. (g) Ohkuma, T.; Koizumi, M.; Doucet, H.; Pham, T.; Kozawa, M.; Murata, K.; Katayama, E.; Yokozawa, T.; Ikariya, T.; Noyori, R. *J. Am. Chem. Soc.* **1998**, *120*, 13529.

(2) DPEN = 1,2-diphenylethylenediamine; TolBINAP = 2,2′-bis(di-4-tolylphosphino)-1,1′-binaphthyl; XylBINAP = 2,2′-bis-(di-3,5-xylyl-phosphino)-1,1′-binaphthyl; DAIPEN = 1,1-di(4-anisyl)-2-isopropyl-1,2-ethylenediamine; DAIPENA = anion of DAIPEN at the 2-position of an anisyl group.

(3) Matsumura, K.; Arai, N.; Hori, K.; Saito, T.; Sayo, N.; Ohkuma, T. *J. Am. Chem. Soc.* **2011**, *133*, 10696.

(4) (a) Etayo, P.; Vidal-Ferran, A. *Chem. Soc. Rev.* **2013**, *42*, 728. (b) Imamoto, T. In *Hydrogenation*; Karamé, I., Ed.; InTech: Croatia, 2012; p 3. (c) Gridnev, I. D.; Imamoto, T. *Chem. Commun.* **2009**, 7447. (d) Knowles, W. S.; Noyori, R. *Acc. Chem. Res.* **2007**, *40*, 1238. (e) Gridnev, I. D.; Imamoto, T. *Acc. Chem. Res.* **2004**, *37*, 633.

(5) (a) Noyori, R. *Angew. Chem., Int. Ed.* **2002**, *41*, 2008. (b) Noyori, R.; Ohkuma, T. *Angew. Chem., Int. Ed.* **2001**, *40*, 40. (c) Noyori, R.; Koizumi, M.; Ishii, D.; Ohkuma, T. *Pure Appl. Chem.* **2001**, *73*, 227. (d) Noyori, R.; Ohkuma, T. *Pure Appl. Chem.* **1999**, *71*, 1493.

(6) Ohkuma, T.; Koizumi, M.; Muñiz, K.; Hilt, G.; Kabuto, C.; Noyori, R. *J. Am. Chem. Soc.* **2002**, *124*, 6508.

(7) Sandoval, C. A.; Ohkuma, T.; Muniz, K.; Noyori, R. *J. Am. Chem. Soc.* **2003**, *125*, 13490.

(8) Magano, J.; Dunetz, J. R. *Org. Process Res. Dev.* **2012**, *16*, 1156.

(9) Chen, C.-y.; Frey, L. F.; Shultz, S.; Wallace, D. J.; Marcantonio, K.; Payack, J. F.; Vazquez, E.; Springfield, S. A.; Zhou, G.; Liu, P.; Kieczykowski, G. R.; Chen, A. M.; Phenix, B. D.; Singh, U.; Strine, J.; Izzo, B.; Krska, S. W. *Org. Process Res. Dev.* **2007**, *11*, 616.

(10) Noyori, R.; Sandoval, C. A.; Muniz, K.; Ohkuma, T. *Philos. Trans. R. Soc., A* **2005**, *363*, 901.

(11) Hamilton, R. J.; Bergens, S. H. *J. Am. Chem. Soc.* **2006**, *128*, 13700.

(12) (a) Hartmann, R.; Chen, P. *Adv. Synth. Catal.* **2003**, *345*, 1353. (b) Hartmann, R.; Chen, P. *Angew. Chem., Int. Ed.* **2001**, *40*, 3581.

(13) Sandoval, C. A.; Yamaguchi, Y.; Ohkuma, T.; Kato, K.; Noyori, R. *Magn. Reson. Chem.* **2006**, *44*, 66.

(14) Noyori, R.; Kitamura, M.; Ohkuma, T. *Proc. Natl. Acad. Sci. U.S.A.* **2004**, *101*, 5356.

(15) (a) Zimmer-De, I. M.; Morris, R. H. *J. Am. Chem. Soc.* **2009**, *131*, 11263. (b) Abdur-Rashid, K.; Clapham, S. E.; Hadzovic, A.; Harvey, J. N.; Lough, A. J.; Morris, R. H. *J. Am. Chem. Soc.* **2002**, *124*, 15104. (c) Abdur-Rashid, K.; Faatz, M.; Lough, A. J.; Morris, R. H. *J. Am. Chem. Soc.* **2001**, *123*, 7473. (d) Abdur-Rashid, K.; Lough, A. J.; Morris, R. H. *Organometallics* **2001**, *20*, 1047.

(16) (a) Štefane, B.; Požgan, F. *Catal. Rev.* **2014**, *56*, 82. (b) Kubas, G. J. *J. Organomet. Chem.* **2014**, *751*, 33. (c) Appel, A. M.; Bercaw, J. E.; Bocarsly, A. B.; Dobbek, H.; DuBois, D. L.; Dupuis, M.; Ferry, J. G.; Fujita, E.; Hille, R.; Kenis, P. J. A.; Kerfeld, C. A.; Morris, R. H.; Peden, C. H. F.; Portis, A. R.; Ragsdale, S. W.; Rauchfuss, T. B.; Reek, J. N. H.; Seefeldt, L. C.; Thauer, R. K.; Waldrop, G. L. *Chem. Rev.* **2013**, *113*, 6621. (d) Zhao, B.; Han, Z.; Ding, K. *Angew. Chem., Int. Ed.* **2013**, *52*, 4744. (e) Eisenstein, O.; Crabtree, R. H. *New J. Chem.* **2013**, *37*, 21.

(17) (a) Sheeba, M. M.; Muthu Tamizh, M.; Farrugia, L. J.; Endo, A.; Karvembu, R. *Organometallics* **2014**, *33*, 540. (b) Faza, O. N.; Fernandez, I.; Lopez, C. S. *Chem. Commun.* **2013**, *49*, 4277. (c) Feng, R.; Xiao, A.; Zhang, X.; Tang, Y.; Lei, M. *Dalton Trans.* **2013**, *42*, 2130. (d) Faza, O. N.; López, C. S.; Fernández, I. *J. Org. Chem.* **2013**, *78*, 5669. (e) Arai, N.; Satoh, H.; Utsumi, N.; Murata, K.; Tsutsumi, K.; Ohkuma, T. *Org. Lett.* **2013**, *15*, 3030. (f) Zuo, W.; Lough, A. J.; Li, Y. F.; Morris, R. H. *Science* **2013**, *342*, 1080. (g) Darwish, M. O.; Wallace, A.; Clarkson, G. J.; Wills, M. *Tetrahedron Lett.* **2013**, *54*, 4250. (h) Zhang, X.; Guo, X.; Chen, Y.; Tang, Y.; Lei, M.; Fang, W. *Phys. Chem. Chem. Phys.* **2012**, *14*, 6003. (i) Chen, H.-Y. T.; Di, T. D.; Hogarth, G.; Catlow, C. R. A. *Dalton Trans.* **2012**, *41*, 1867. (j) Perry, R. H.; Brownell, K. R.; Chingin, K.; Cahill, T. J.; Waymouth, R. M.; Zare, R. N. *Proc. Natl. Acad. Sci. U.S.A.* **2012**, *109*, 2246.

(18) Hedberg, C.; Kaellstroem, K.; Arvidsson, P. I.; Brandt, P.; Andersson, P. G. *J. Am. Chem. Soc.* **2005**, *127*, 15083.

(19) (a) Chen, H.-Y. T.; Di, T. D.; Hogarth, G.; Catlow, C. R. A. *Catal. Lett.* **2011**, *141*, 1761. (b) Di, T. D.; French, S. A.; Catlow, C. R. A. *J. Mol. Struct. (THEOCHEM)* **2007**, *812*, 39. (c) Leyssens, T.; Peeters, D.; Harvey, J. N. *Organometallics* **2008**, *27*, 1514.

(20) Hasanayn, F.; Morris, R. H. *Inorg. Chem.* **2012**, *51*, 10808.

(21) (a) Kozuch, S. *ACS Catal.* **2013**, *3*, 380. (b) Lente, G. *ACS Catal.* **2013**, *3*, 381. (c) Kozuch, S.; Martin, J. M. L. *ACS Catal.* **2012**, *2*, 2787. (d) Herrmann, W. A.; Cornils, B. *Angew. Chem., Int. Ed. Engl.* **1997**, *36*, 1048.

(22) (a) Takebayashi, S.; Dabral, N.; Miskolzie, M.; Bergens, S. H. *J. Am. Chem. Soc.* **2011**, *133*, 9666. (b) Hamilton, R. J.; Bergens, S. H. *J. Am. Chem. Soc.* **2008**, *130*, 11979. (c) Hamilton, R. J.; Leong, C. G.; Bigam, G.; Miskolzie, M.; Bergens, S. H. *J. Am. Chem. Soc.* **2005**, *127*, 4152.

(23) Kitamura, M.; Nakatsuka, H. *Chem. Commun.* **2011**, *47*, 842.

(24) (a) Chen, H.-Y. T.; Di, T. D.; Hogarth, G.; Catlow, C. R. A. *Dalton Trans.* **2011**, *40*, 402. (b) Di Tommaso, D.; French, S. A.; Zanotti-Gerosa, A.; Hancock, F.; Palin, E. J.; Catlow, C. R. A. *Inorg. Chem.* **2008**, *47*, 2674. (c) French, S. A.; Di, T. D.; Zanotti-Gerosa, A.; Hancock, F.; Catlow, C. R. A. *Chem. Commun.* **2007**, 2381.

(25) Chen, Y.; Tang, Y.; Lei, M. *Dalton Trans.* **2009**, *0*, 2359.

(26) Dub, P. A.; Ikariya, T. *J. Am. Chem. Soc.* **2013**, *135*, 2604.

(27) (a) Pavlova, A.; Meijer, E. J. *ChemPhysChem* **2012**, *13*, 3492. (b) Handgraaf, J.-W.; Meijer, E. J. *J. Am. Chem. Soc.* **2007**, *129*, 3099.

(28) Otsuka, T.; Ishii, A.; Dub, P. A.; Ikariya, T. *J. Am. Chem. Soc.* **2013**, *135*, 9600.

(29) It was important to use the real catalyst structures in the computations, because it is known experimentally that even slight simplifications of catalyst structure can result in significant losses in activity and enantioface selectivity.

(30) Frisch, M. J. *Gaussian 09*, revision C.01; Gaussian, Inc.: Pittsburgh, PA, 2009.

(31) Marenich, A. V.; Cramer, C. J.; Truhlar, D. G. *J. Phys. Chem. B* **2009**, *113*, 6378.

(32) (a) Hohenberg, P.; Kohn, W. *Phys. Rev.* **1964**, *136*, B864. (b) Kohn, W.; Sham, L. J. *Phys. Rev.* **1965**, *140*, A1133.

(33) Chai, J.-D.; Head-Gordon, M. *Phys. Chem. Chem. Phys.* **2008**, *10*, 6615.

(34) Reichardt, C.; Welton, T. *Solvents and Solvent Effects in Organic Chemistry*, 4th ed.; Wiley-VCH: New York, 2010.

(35) Dewar, M. J. S. *J. Am. Chem. Soc.* **1984**, *106*, 209.

(36) Bertoli, M.; Choualeb, A.; Lough, A. J.; Moore, B.; Spasyuk, D.; Gusev, D. G. *Organometallics* **2011**, *30*, 3479.

(37) Chen, Y.; Liu, S.; Lei, M. *J. Phys. Chem. C* **2008**, *112*, 13524.

(38) (a) Elm, J.; Bilde, M.; Mikkelsen, K. V. *Phys. Chem. Chem. Phys.* **2013**, *15*, 16442. (b) Liu, Y.; Zhao, J.; Li, F.; Chen, Z. *J. Comput. Chem.* **2013**, *34*, 121. (c) Vydrov, O. A.; Van Voorhis, T. *J. Chem. Theory Comput.* **2012**, *8*, 1929. (d) Thanthiriwatte, K. S.; Hohenstein, E. G.; Burns, L. A.; Sherrill, C. D. *J. Chem. Theory Comput.* **2010**, *7*, 88. (e) Yang, K.; Zheng, J.; Zhao, Y.; Truhlar, D. G. *J. Chem. Phys.* **2010**, *132*, 164117. (f) Kang, Y. K.; Byun, B. J. *J. Comput. Chem.* **2010**, *31*, 2915.

(39) The optimization with 6-311++G** was extremely slow even if a supercomputer resources were applied.

(40) Inspecting the relative energy profiles reveals that both transition states and intermediates shown in Figures 1 and 3 are deeper lying by an average value of 3−5 kcal mol^{-1} (ΔE) using SDD +f(Ru)/6-311++G**(C,H,N,O,P,K)//SDD(Ru)/6-31G*(C,H,N,O,P,K), whereas the average relative activation barriers for single steps and energy difference between intermediates are 2 and 4 kcal mol^{-1} ($\Delta \Delta E$), respectively. The highest average discrepancy of ~4 kcal mol^{-1} was observed for structures in Figure 5. This is expected, because these transition states are characterized by both high charge separation/distribution and the presence of ionic N−K bonds. The energy difference is probably due to the presence/absence of diffusion functions that are necessary to allow angular and radial flexibility of the ionic species.

(41) (a) Pegado, L.; Marsalek, O.; Jungwirth, P.; Wernersson, E. *Phys. Chem. Chem. Phys.* **2012**, *14*, 10248. (b) Lund, M.; Jagoda-Cwiklik, B.; Woodward, C. E.; Vácha, R.; Jungwirth, P. *J. Phys. Chem. Lett.* **2009**, *1*, 300. (c) Contreras, R. R.; Padilla, L.; Gomez-Jeria, J. S.; Aizman, A. J. *THEOCHEM* **1990**, *69*, 147.

(42) Bernales, V. S.; Marenich, A. V.; Contreras, R.; Cramer, C. J.; Truhlar, D. G. *J. Phys. Chem. B* **2012**, *116*, 9122.

(43) According to several authors, that is, ref 44a, the frequencies are calculated in the dielectric continuum and the 1 M standard state (SMD model). After exchanging several emails with Gaussian Technical Support, it appears, however, that the standard state concentration for this part of the output is 1 atm.

(44) (a) Di Tommaso, D. *CrystEngComm* **2013**, *15*, 6564. (b) Marenich, A. V.; Ding, W. D.; Cramer, C. J.; Truhlar, D. G. *J. Phys. Chem. Lett.* **2012**, *3*, 1437. (c) Ribeiro, R. F.; Marenich, A. V.; Cramer, C. J.; Truhlar, D. G. *J. Phys. Chem. B* **2011**, *115*, 14556. (d) Kim, Y.; Mohrig, J. R.; Truhlar, D. G. *J. Am. Chem. Soc.* **2010**, *132*, 11071. (e) Ho, J.; Klamt, A.; Coote, M. L. *J. Phys. Chem. A* **2010**, *114*, 13442. (f) Guthrie, J. P.; Povar, I. *Can. J. Chem.* **2009**, *87*, 1154. (g) Winget, P.; Cramer, C. J.; Truhlar, D. G. *Theor. Chem. Acc.* **2004**, *112*, 217.

(45) Fukui, K. *Acc. Chem. Res.* **1981**, *14*, 363.

(46) Pettersen, E. F.; Goddard, T. D.; Huang, C. C.; Couch, G. S.; Greenblatt, D. M.; Meng, E. C.; Ferrin, T. E. *J. Comput. Chem.* **2004**, *25*, 1605.

(47) Amatore, C.; Jutand, A. *J. Organomet. Chem.* **1999**, *576*, 254.

(48) Kozuch, S.; Shaik, S. *Acc. Chem. Res.* **2010**, *44*, 101.

(49) Noyori, R. *CHEMTECH* **1992**, *22*, 360.

(50) (a) Espinet, P.; Casares, J. A. *Phys. Organomet. Chem.* **2004**, *4*, 131. (b) Espinet, P.; Casares, J. A. In *Fluxional Organometallic and Coordination Compounds*; Gielen, M., Willem, R., Wrackmeyer, B., Eds.; Wiley & Sons, Ltd.: New York, 2004; Vol. 4, p 131.

(c) Buckingham, D. A.; Sargeson, A. M. *Topics in Stereochemistry*; John Wiley & Sons, Inc.: New York, 2007; p 219.

(51) Coe, B. J.; Glenwright, S. J. *Coord. Chem. Rev.* **2000**, *203*, 5.

(52) Macchioni, A. *Chem. Rev.* **2005**, *105*, 2039.

(53) (a) Belkova, N. V.; Epstein, L. M.; Shubina, E. S. *Arkivoc* **2008**, *IV*, 120. (b) Belkova, N. V.; Shubina, E. S.; Epstein, L. M. *Acc. Chem. Res.* **2005**, *38*, 624. (c) Brammer, L. *Dalton Trans.* **2003**, 3145. (d) Epstein, L. M.; Shubina, E. S. *Coord. Chem. Rev.* **2002**, *231*, 165. (e) Calhorda, M. J. *Chem. Commun.* **2000**, 801.

(54) For 4^{OSIP}, geometry optimization was performed with a 5% increase in atomic radii size used to build the solute cavity (the solute cavity that the program built with the default SMD option resulted a numerical instability in the PCM calculation). As this procedure changed the energy, the energy difference between 4^{OSIP} and 4^{ISIP} was calculated taking into account the energy difference for complex 6, optimized under default SMD calculations and with a 5% increase in atomic radii.

(55) (a) Filippov, O. A.; Belkova, N. V.; Epstein, L. M.; Lledos, A.; Shubina, E. S. *ChemPhysChem* **2012**, *13*, 2677. (b) Belkova, N. V.; Epstein, L. M.; Shubina, E. S. *Eur. J. Inorg. Chem.* **2010**, 3555. (c) Crabtree, R. H.; Eisenstein, O.; Sini, G.; Peris, E. *J. Organomet. Chem.* **1998**, *567*, 7.

(56) ACD/Labs 6.00 predicts the pK_a for phenylethanol as pK_a = 14.43 ± 0.20, whereas for propan-2-ol pK_a = 15.31 ± 0.20 under its default parameters.

(57) A transition state similar to TS$_6$ has been calculated by López and co-workers (ref 17b), where it was proposed to be an entry point to the catalytic cycle II in Scheme 1.

(58) The more facile heterolytic activation of H$_2$ via TS$_5$ and TS$_6$ (~1 kcal mol^{-1}) rather than via TS$_7$ (relative activation energy $\Delta \Delta G°_{298K}$‡ = 8.6 kcal mol^{-1} for the single step 11 → TS$_7$) is probably due to the more electron-deficient nature of the metal center in 7 and 9, respectively.

(59) Kubas, G. J. *Chem. Rev.* **2007**, *107*, 4152.

(60) John, J. M.; Takebayashi, S.; Dabral, N.; Miskolzie, M.; Bergens, S. H. *J. Am. Chem. Soc.* **2013**, *135*, 8578.

(61) Dougherty, D. A. *Science* **1996**, *271*, 163.

(62) (a) Wible, B. A.; Brown, A. M. *Drug Dev. Res.* **1994**, *33*, 225. (b) Miller, C. *Science* **1991**, *252*, 1092.

(63) Fache, E.; Santini, C.; Senocq, F.; Basset, J. M. *J. Mol. Catal.* **1992**, *72*, 337.

(64) Junge, K.; Wendt, B.; Addis, D.; Zhou, S.; Das, S.; Fleischer, S.; Beller, M. *Chem.—Eur. J.* **2011**, *17*, 101.

(65) Västilä, P.; Zaitsev, A. B.; Wettergren, J.; Privalov, T.; Adolfsson, H. *Chem.—Eur. J.* **2006**, *12*, 3218.

(66) Yamada, S.; Morita, C. *J. Am. Chem. Soc.* **2002**, *124*, 8184.

(67) (a) Zhou, X.; Kay, S.; Toney, M. D. *Biochemistry* **1998**, *37*, 5761. (b) Toney, M.; Hohenester, E.; Cowan, S.; Jansonius, J. *Science* **1993**, *261*, 756.

(68) (a) Kuniyil, R.; Sunoj, R. B. *Org. Lett.* **2013**, *15*, 5040. (b) Andrews, P. C.; Blair, V. L.; Border, E. C.; Peatt, A. C.; MacLellan, J. G.; Thompson, C. D. *Organometallics* **2013**, *32*, 7509. (c) Um, I.-H.; Shin, Y.-H.; Lee, S.-E.; Yang, K.; Buncel, E. *J. Org. Chem.* **2008**, *73*, 923.

(69) (a) Dougherty, D. A. *Acc. Chem. Res.* **2012**, *46*, 885. (b) Mahadevi, A. S.; Sastry, G. N. *Chem. Rev.* **2012**, *113*, 2100. (c) Meot-Ner, M. *Chem. Rev.* **2012**, *112*, PR22. (d) Schneider, H.-J. *Acc. Chem. Res.* **2012**, *46*, 1010. (e) Wheeler, S. E.; Houk, K. N. *J. Am. Chem. Soc.* **2009**, *131*, 3126. (f) Tsuzuki, S.; Yoshida, M.; Uchimaru, T.; Mikami, M. *J. Phys. Chem. A* **2001**, *105*, 769. (g) Ma, J. C.; Dougherty, D. A. *Chem. Rev.* **1997**, *97*, 1303. (h) Smith, J. M.; Lachicotte, R. J.; Pittard, K. A.; Cundari, T. R.; Lukat-Rodgers, G.; Rodgers, K. R.; Holland, P. L. *J. Am. Chem. Soc.* **2001**, *123*, 9222.

(70) (a) Kuriyama, W.; Matsumoto, T.; Ino, Y.; Ogata, O. Patent WO2011048727A1; Takasago International Corp.: Japan, 2011. (b) Kuriyama, W.; Matsumoto, T.; Ogata, O.; Ino, Y.; Aoki, K.; Tanaka, S.; Ishida, K.; Kobayashi, T.; Sayo, N.; Saito, T. *Org. Process Res. Dev.* **2011**, *16*, 166.

3520

dx.doi.org/10.1021/ja411374j | *J. Am. Chem. Soc.* 2014, 136, 3505−3521

(71) (a) Goussev, D.; Spasyuk, D. Can. Patent WO2013023307A1, 2013. (b) Spasyuk, D.; Smith, S.; Gusev, D. G. *Angew. Chem., Int. Ed.* **2012**, *51*, 2772.

(72) Spasyuk, D.; Smith, S.; Gusev, D. G. *Angew. Chem., Int. Ed.* **2013**, *52*, 2538.

(73) Dub, P. A.; Ikariya, T. *ACS Catal.* **2012**, *2*, 1718.

(74) (a) Patchett, R.; Magpantay, I.; Saudan, L.; Schotes, C.; Mezzetti, A.; Santoro, F. *Angew. Chem., Int. Ed.* **2013**, *52*, 10352. (b) Santoro, F.; Saudan, L. Patent WO2012084810A1, 2012. (c) Yang, X.-H.; Xie, J.-H.; Liu, W.-P.; Zhou, Q.-L. *Angew. Chem., Int. Ed.* **2013**, *52*, 7833.

(75) Tesh, K. F.; Hanusa, T. P.; Huffman, J. C. *Inorg. Chem.* **1990**, *29*, 1584.

(76) Domingos, A. M.; Sheldrick, G. M. *Acta Crystallogr., Sect. B* **1974**, *30*, 517.

(77) (a) Glock, C.; Younis, F. M.; Ziemann, S.; Görls, H.; Imhof, W.; Krieck, S.; Westerhausen, M. *Organometallics* **2013**, *32*, 2649. (b) Johns, A. M.; Chmely, S. C.; Hanusa, T. P. *Inorg. Chem.* **2009**, *48*, 1380.

(78) Strictly speaking, there is no naked K$^+$ ion because the potassium is bound to a nitrogen atom via a bond with a presumably high ionic contribution and the overall complex is neutral. Nevertheless, we will be using the term "cation−π" in this work to underline the interaction.

(79) In Figure 6 only one is shown, for the sake of clarity.

(80) In fact, the activation barrier of the enantiodetermining hydride transfer is also reduced by ∼1−2 kcal mol^{-1}. However, this energy difference is within the typical accuracy (noise) of the DFT method. On the other hand, increase in the reaction rate by 1 order of magnitude as was experimentally observed in the presence of base excess corresponds to the lowering of the $\Delta G_{298K}^{\circ}{}_{cycle}$ by 1.36 kcal mol^{-1}.

(81) We estimate the accuracy of the free energy calculations as at least ±3−4 kcal mol^{-1}.

(82) (a) Gregory, M. C.; Denisov, I. G.; Grinkova, Y. V.; Khatri, Y.; Sligar, S. G. *J. Am. Chem. Soc.* **2013**, *135*, 16245. (b) Zhang, D.; Kovach, I. M. *Biochemistry* **2006**, *45*, 14175. (c) Tinsley, R. A.; Harris, D. A.; Walter, N. G. *J. Am. Chem. Soc.* **2003**, *125*, 13972. (d) Northrop, D. B. *Annu. Rev. Biochem.* **1981**, *50*, 103.

(83) (a) Limbach, H. H.; Miguel Lopez, J.; Kohen, A. *Philos. Trans. R. Soc., B* **2006**, *361*, 1399. (b) Miyazaki, T. *J. Nucl. Sci. Technol.* **2002**, *39*, 339. (c) Krishtalik, L. I. *Biochim. Biophys. Acta* **2000**, *1458*, 6. (d) Christov, S. G. *Chem. Phys.* **1992**, *168*, 327.

(84) The corresponding stationary point corresponds to the most stable found Ru alkoxo monoamidato complex.

(85) Taking into account "accuracy" of the DFT, see footnotes 80 and 81.

(86) Truhlar, D. G.; Garrett, B. C. *J. Am. Chem. Soc.* **1989**, *111*, 1232.

(87) It appears that the measured (and calculated) KIE, as a matter of fact, not a kinetic effect proper, but reflects the thermodynamics of the reaction acetophenone + H$_2$ = (*R*)-C$_6$H$_5$CH(OH)CH$_3$ versus acetophenone + D$_2$ = (*R*)-C$_6$H$_5$CD(OD)CH$_3$.

(88) Pietsch, M. A.; Russo, T. V.; Murphy, R. B.; Martin, R. L.; Rappé, A. K. *Organometallics* **1998**, *17*, 2716.

(89) (a) Dub, P. A.; Poli, R. *J. Mol. Catal. A* **2010**, *324*, 89. (b) Singh, N.; Warshel, A. *J. Phys. Chem. B* **2009**, *113*, 7372. (c) Chipot, C., Pohorille, A., Eds. Free Energy Calculations: Theory and Applications in Chemistry and Biology. *Springer Series in Chemical Physics*; Springer GmbH: New York, 2007; Vol. 86. (d) Carlsson, J.; Aqvist, J. *J. Phys. Chem. B* **2005**, *109*, 6448. (e) Chang, C. E.; Chen, W.; Gilson, M. K. *J. Chem. Theory Comput.* **2005**, *1*, 1017.

(90) The energy difference between transition states leading to the minor *S*-enantiomer and the major *R*-enantiomer (or correspondingly enantioselectivity, ee %) was calculated as ΔE (kcal mol^{-1}) = $-([\ln(\nu_S/\nu_R)]\cdot 0.58$ kcal mol^{-1}), 0.58 kcal mol^{-1} = RT (ν_S and ν_R are reaction rates leading to the *S*-enantiomer and the *R*-enantiomer, respectively). $\nu_R + \nu_S = 100$, $\nu_R - \nu_S = $ ee, %. From these three equations, one may obtain ee, % = $100*[\{2/(1 + \exp(-\Delta E/RT))\} - 1]$.

(91) RT = 0.58 kcal mol^{-1}.

(92) Sandoval, C. A.; Shi, Q.; Liu, S.; Noyori, R. *Chem.-Asian J.* **2009**, *4*, 1221.

(93) The reaction occurs facilely with 2,2,2-trifluoroacetophenone or benzophenone derivatives, confirming that the C=O function is hydrogenated rather than taking the enol form. See refs 1g and 94, respectively.

(94) Ohkuma, T.; Koizumi, M.; Ikehira, H.; Yokozawa, T.; Noyori, R. *Org. Lett.* **2000**, *2*, 659.

(95) Sastre de Vicente, M. E. *J. Chem. Educ.* **2004**, *81*, 750.

(96) (a) Berkessel, A.; Schubert, T. J. S.; Müller, T. N. *J. Am. Chem. Soc.* **2002**, *124*, 8693. (b) Walling, C.; Bollyky, L. *J. Am. Chem. Soc.* **1964**, *86*, 3750. (c) Walling, C.; Bollyky, L. *J. Am. Chem. Soc.* **1961**, *83*, 2968.

(97) *tert*-Butyl alcohol somewhat retarded hydrogenation in 2-propanol: the initial velocity for acetophenone hydrogenation by **1f** steadily decreases with increasing *tert*-butyl alcohol content for 2-propanol/*tert*-butyl alcohol solvent mixtures; see ref 7.

(98) Harder, S. *Coord. Chem. Rev.* **1998**, *176*, 17.

(99) Gordon, J. C.; Kubas, G. J. *Organometallics* **2010**, *29*, 4682.

(100) *Topics in Organometallic Chemistry: Bifunctional Molecular Catalysis*; Ikariya, T., Shibasaki, M., Eds.; Springer: New York, 2011; Vol. 37.